UNIVERSITÀ DEGLI STUDI DI PADOVA

DIPARTIMENTO DI INGEGNERIA INDUSTRIALE

CORSO DI LAUREA MAGISTRALE IN INGEGNERIA DEI MATERIALI

Tesi di Laurea Magistrale in Ingegneria dei Materiali

Structured ammonia sorbents fabricated by direct ink writing of strontium chloride based composites

Relatore Prof. Giorgia Franchin
Co-Relatore Dr. Marco Lorenzo D'Agostini

Laureando
Ali Ezzine 1241489

A.A. 2021-2022

UNIVERSITÀ DEGLI STUDI DI PADOVA

DIPARTIMENTO DI INGEGNERIA INDUSTRIALE

CORSO DI LAUREA MAGISTRALE IN INGEGNERIA DEI MATERIALI

Tesi di Laurea Magistrale in Ingegneria dei Materiali

Structured ammonia sorbents fabricated by direct ink writing of strontium chloride based composites

Relatore Prof. Giorgia Franchin
Co-Relatore Dr. Marco Lorenzo D'Agostini

Laureando
Ali Ezzine 1241489

A.A. 2021-2022

Abstract

As air and environmental pollution steadily get worse, mankind struggles to find a long term solution, while attempting to at least alleviate the issue by employing a wide array of techniques. One such tool are absorption devices, cost-effective and efficient tools for purification and filtration. Using recently discovered specific materials, it becomes possible to collect pollutant from their surroundings and potentially reuse it. Among the widely employed absorption tools, we find alkaline metal halides, an helpful solution for storing ammonia in Selective Catalytic Reduction devices (SCR), used to cull nitrogen oxide produced in car engines. As these salts can not be used in technical applications on their own, they have been matched and mixed with other materials acting as binders to overcome such intrinsic downfalls. This work investigates the coupling of strontium chloride and sodium bentonite specifically.

Additive manufacturing is a production technique that emerged in recent years, with very broad and multidisciplinary applications, in this producing high surface area structures for absorption purposes. A porous strontium chloride-bentonite scaffold was fabricated through Direct Ink Writing (DIW), a branch of Additive Manufacturing. The morphological characteristics and mechanical behavior of 3D printed sorbents were evaluated for feasible applications. Experiments have been carried out to investigate the effects of different compositions, and the overall performance of the structure. The results offer a possible solution for ammonia carriers in SCR systems and in ammonia storage as structured Strontium Chloride composites give good absorption-desorption properties and enhanced structural stability.

Contents

CHAPTER 1

Introduction

1.1 Air pollution

The overall motivation for having clean air is: first for health reasons and second to stop or at least slow down the problem of environmental pollution. There are essentially only two general methods for ensuring it: application of control technologies that clean air by the removal of pollutants, and methods of prevention. As a general rule of thumb, prevention is more costeffective than the application of so called end of pipe treatment technologies. However, there are many situations where control technologies represent the only feasible methods to managing air pollution problems. Only one approach is presented in this work, and in general we need to assess which is the most appropriate means on a case by case basis. [1]

Nitrogen oxides (NO_x), including nitric oxide (NO) and NO_2, is one of the six "criteria air pollutants" according to the United States (U.S.) Environment Protection Agency (EPA), this oxides are listed as the main pollutant of the air quality indices/indicators in many countries and regions, such as China and Europe, due to the devastating environmental impact of NO_x. Nitrogen oxides are released to the air from the exhaust of motor vehicles, the burning of coal, oil, or natural gas, and during processes such as arc welding, electroplating, engraving, and dynamite blasting and they are also produced commercially. From a health perspective, low levels of nitrogen oxides in the air can irritate eyes, nose, throat, and lungs, possibly causing cough and shortness of breath, tiredness, and nausea. Exposure to low levels can also result in fluid build-up in the lungs one or two days after exposure. Nonetheless breathing high levels of nitrogen oxides is far more dangerous and can cause rapid burning, spasms, and swelling of tissues in the throat and upper respiratory tract, reduced oxygenation of body tissues, a build-up of fluid in your lungs, and eventually death. For an environmental stand point nitrogen dioxide is toxic to plants in short-term concentrations. It reduces plant growth. When sulphur dioxide and ozone are also present, the effects on vegetation are worse. Along with sulphur dioxide, nitrogen dioxide can cause acid rain and contributes to nutrient pollution in coastal waters Therefore, the control of $-NO_x-$ emission has become an urgent and inevitable task. [2]

From an European perspective, EU environmental policy is mostly established by means of directives, imposing environmental objectives to be achieved by the member States. EU Directives fix the framework in which Member States must create national legislation directed to industries/civilians in order to attain the environmental quality objectives laid down in

the directives. Understanding EU policy measures dealing with N emissions abatement requires insight into the understanding and perception by scientists and policy makers of the cause–effect relationships of these emissions. Many current policy measures dealing with N emissions reflect a simple 'source – receptor/ effect' model of understanding. As said before Combustion (mainly (NO_x) by industry, power plants and traffic), waste waters (mainly dissolved and particulate N in discharges by industry and households) and agriculture (diffuse emissions of NH_3 and NO_2 to air and NO_3 to waters) are seen as the main N sources, while atmosphere, surface waters and groundwater are seen as the direct receptors. Thus, many policy measures focus on decreasing N compound emissions from specific sources and/or on decreasing N compound concentrations in receiving bodies (receptors) to below critical concentration levels. For this purpose different devices were designed for reduce the emissions in one some of this sources, an example for car engine is the SCR Selective catalytic reduction. [3][4]

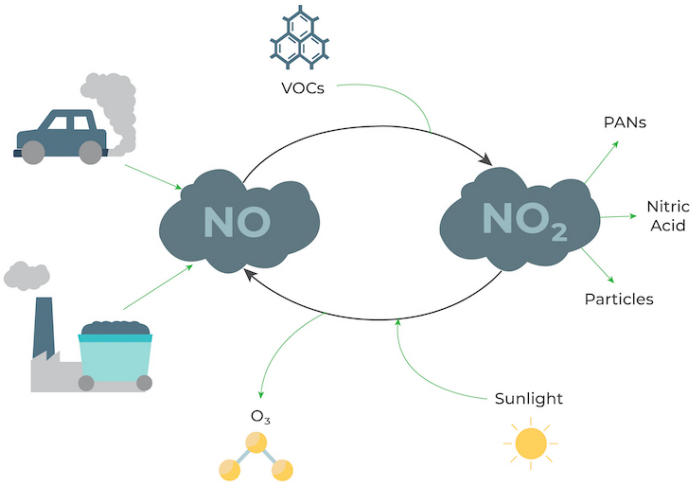

Figure 1.1: NO cycle in the atmosphere

1.2 Selective catalytic reduction (SCR)

For alleviate and control emissions selective catalytic reduction (SCR) has been used to sourced fossil fuel-fired combustion units since the early 1970s and is currently being used in first world countries of Asia, Europe and America. Nowadays most heavy-duty vehicles and some light duty vehicles are equipped with SCR systems to meet emission standards. The main purpose is to de$-NO_x$ the gas emissions of the plants or engines by actively control this product. The major components of a SCR system are:

- Catalyst where the conversion of NO into N_2 takes place ;
- Reductant injection system;
- Particulate filter.

The SCR works as follows: the hot exhaust gases flow out of the engine and into the SCR system where aqueous urea or ammonia (NH_3) (trademarked as AdBlue® in the EU market, and diesel exhaust fluid (DEF) in U.S. market) is sprayed onto a catalyst. The DEF sets off a

chemical reaction in the exhaust on the catalyst that converts nitrogen oxides into nitrogen, water, and a tiny amounts of carbon dioxide CO_2. The exhaust passes through a particulate filter in the system and then is then expelled through the vehicle tailpipe. The design of SCR technology is such that it permits nitrogen oxide (NO_x) reduction reactions to take place in an oxidizing atmosphere and it can be called "selective" because it selectivity reduces levels of NO_x using ammonia as a reductant within a catalyst system. The chemical reaction that happens is known as "reduction" where the DEF is the reducing agent that reacts with NO_x to "reduce" the pollutants into nitrogen, water and in order to introduce NH_3 into the exhaust gas stream, proper dosage control mechanism is required as shown in Fig. 1.2.

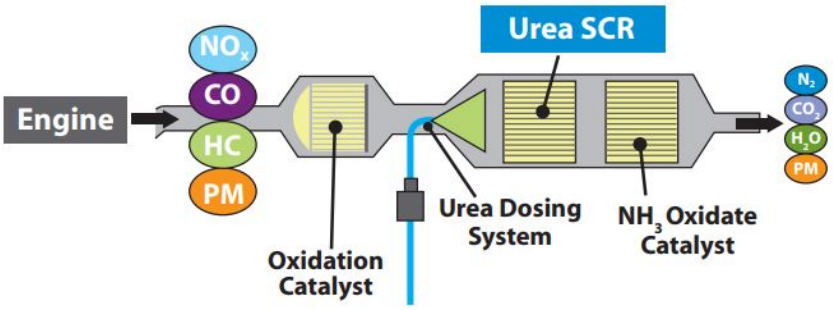

Figure 1.2: Schematics of a SCR system

The reduction reaction that happens in the catalyst are as follows:

$$4NO + 4NH_3 + O_2 \rightarrow 4N_2 + 6H_2O$$

$$NO + NO2 + 2NH_3 \rightarrow 2N2 + 3H2O$$

$$6NO_2 + 8NH_3 \rightarrow 7N_2 + 12H_2O$$

The major challenge involved with this type of systems are related to the reduction of catalytic converter volume at low temperatures and the suitable dosing strategy for NH_3 at frequently varying load conditions of the diesel engines. Additionally, the risk associated concerning storing and handling of gaseous NH_3 is significant and consequentially it is not commonly used as a reducing agent directly and for this reasons urea is the preferred substitute for NH_3 as reducing agent. Handling of NH_3 has to be accurate and it is required to be stored at high pressure. Urea is an environmentally benign chemical which makes it more suitable for application to the SCR process even from an environmental stand point. Urea is used as a fertilizer in agriculture and available in a number of quality grades at a low cost. Development of Urea-SCR over NH_3-SCR has gained momentum due to various problems involved with the use of NH_3.

The main advantage with this SCR system (both ammonia and urea) is high De$-NO_x$ efficiency (90% or higher) while the disadvantages involve the space required for the catalyst, high capital- and operating costs, formation of other emissions (NH_3 slip) and formation of undesirable species which may lead to catalyst poisoning and deactivation, but for what we know the NH_3 slip can be controlled by installing an oxidation catalyst after the SCR system. Although the SCR system has some drawbacks the technology has been chosen by the majority of the diesel engine manufactures due to absence of better technology to meet the stringent emission standards. [5] As we understand the reducing agent is the core of the SCR and therefore different ways of introduce it to the system were implemented; it can be delivered as anhydrous NH_3, aqueous NH_3 or an aqueous urea solution that decomposes to NH_3. It has been shown that best SCR performance is obtained by gaseous NH_3, followed by injection of a NH_3 solution. The performance with solid urea and urea solution is comparatively poor

due to incomplete evaporation and decomposition of urea.[6] Before the use of NH_3 or urea different reducing agents were tested, one of them are hydrocarbon reductants (methane, alcohol, etc.), molecular hydrogen (H_2), carbon oxide (CO). Hydrocarbon reductants require effective catalysts to meet the NO_x conversion rate. H_2 as a reductant can produce undesired N_2O and requires an onboard H_2 tank. CO can be oxidized into CO_2, resulting in a failure in NO_x conversion. Therefore, ammonia reductants become dominant in SCR systems. Since then, ammonia production has increased continuously and nowadays, ammonia is one of the most produced base chemicals for this and other reasons.

Figure 1.3: AdBlue®, DEF reservoir [7]

Nowadays some emerging problems in the urea-based SCR have recently constrained the SCR system to meet future emission standards. For instance, lowering of exhaust temperature. To tackle this new standards novel reductant systems have been investigated and applied both in research and industry. One of them are alkaline earth metal halides (AEMHs), such as $MgCl_2$, $CaCl_2$, and $SrCl_2$, which have recently emerged as a research hotspot in SCR reductants because of for their capability to form complexes with ammonia and other numerous advantages, including lower exhaust temperature requirements (operating temperature below 100 °C, compared with 200 °C of ammonia based reductant), high ammonia capacity both gravimetrically and volumetrically, and excellent ammonia-recharge and cyclic performance. In using this type of materials, the ammonia, instead of being kept in a gaseous phase, it is stored in the form of metal ammine complexes with AEMHs, such as $Mg(NH_3)_6Cl_2$, $Ca(NH_3)_8Cl_2$, and $Sr(NH_3)_8Cl_2$.

$$SrCl_2 + NH_3 \rightarrow Sr(NH_3)_8Cl_2$$

$$Sr(NH_3)Cl_2 \rightarrow SrCl_2 + NH_3$$

To give an exemplified way to understand how the equilibrium reaction of the ammonia sorption in AEMHs happens, we can deduce that it follows the Van't Hoff equation, (referred to as the Clausius–Clapeyron relation in some literature), proposed by Jacobus Henricus van't Hoff, the first winner of the Nobel Prize in Chemistry 1901, the Hoff equation has been widely utilized to explore the changes in state functions in a thermodynamic system and the releatedd van 't Hoff plot, which is derived from this equation, is especially effective in estimating the change in enthalpy, or total energy, and entropy, or amount of disorder, of a chemical reaction. The equation is characterized by different parameters: Peq is the equilibrium pressure (Pa), H the enthalpy change, S the entropy change and R the universal

gas constant. [8]

$$ln(\frac{P_{eq}}{Pa}) = -\frac{-\Delta H}{RT} + \frac{\Delta S}{R}$$

And for our case study with the changes in temperature or pressure, metal ammine complexes can form and decompose, offering direct ammonia absorption and desorption.

1.3 Alkaline earth metal halides - Strontium Chloride

Alkaline earth metal halides (AEMHs) are one of the most common ammonia carriers and consist of halogen anions and alkaline earth metal cations. The name "alkaline earth" comes from alchemist times and relates to their basic oxides, while "alkali" derives from the Arab term for "ashes of the saltwort", saltwort being flowering plants growing in a salty environment. The alkaline earth metal elements Be, Mg, Ca, Sr, Ba, and Ra are all silvery shining metals with an ns^2 electronic configuration. Some of the alkaline earth compounds are known since prehistoric times, like gypsum, limestone or chalk, while others have been discovered between the 17th and the 19th century. Halogens instead are elements in group 17 of the periodic table, including fluorine (F), chlorine (Cl), bromine (Br), iodine (I), and astatine (At). Among them, beryllium forms covalent bonds with Cl instead of ionic bonds, Ba^{2+} is toxic, and Ra is the only one showing radioactive features. Therefore, the most common AEMHs cations are Mg^{2+}, Ca^{2+}, and Sr^{2+}. specially, for ammonia carriers in SCR systems, $MgCl_2$, $CaCl_2$, and $SrCl_2$ are the most widely used due to their high ammonia absorption/desorption capacity, this capability is for each alkaline earth metal cations different, as the number of ammonia molecules which can be absorbed varies. For example,Mg^{2+} can absorb 6 ammonia molecules to obtain $Mg(NH_3)_6Cl_2$, while Ca^{2+}, Sr^{2+}, and Ba^{2+} can absorb 8 ammonia molecules to form $Ba(NH_3)_8Cl_2$, $Ca(NH_3)_8Cl_2$, and $Sr(NH_3)_8Cl_2$ respectively.

As the heat and mass transfer in AEMHs is relatively low, AEMHs are usually applied in composites with some other materials (referred to as matrix), especially in thermal energy storage applications. In SCR applications, AEMHs composites with good heat and mass transfer performance can elevate the kinetics of ammonia dosing as the adsorption and desorption process is thermally activated. The most common matrix for AEMHs as ammonia sorbents is expanded natural graphite (ENG), due to its relatively low cost, good thermal conductivity, low thermal expansion, and anti-corrosion properties. An ENG matrix can significantly enhance the permeability and thermal conductivity, offering an enhanced ammonia absorption and desorption performance. But new matrix are yet to be discovered, as in this work a new one is proposed. There are mainly two approaches to fabricate the AEMHs composites: solid mixture and consolidation, and impregnation with/without consolidation. The solid mixture, using ball milling or a mixer, is a simple method to obtain a raw material that can be implemented for additive manufacturing. Consolidation through compression can be also applied in the impregnation approach to achieve a certain density of the composites. In the next chapters the first method will be used to produce a scaffold with the main material strontium chloride.

There are several challenges in using AEMHs, including $SrCl_2$, as ammonia carriers in structured form. The main one is due to compositional and structural changes during the chemisorption, AEMHs have 400% volume swing during ammonia absorption and desorption related to the molar weight increase, for example, $MgCl_2$ (41 $cm^3\,mol^{-1}$) to $Mg(NH_3)_6Cl_2$ (157 $cm^3\,mol^{-1}$), $SrCl_2$ (52 $cm^3\,mol^{-1}$) to $Sr(NH_3)_8Cl_2$ (212 $cm^3\,mol^{-1}$). During the absorption–desorption cycles, the structured $SrCl_2$ could disintegrate to powder as the result of the large volume change. The nature of the volume swing associated with $SrCl_2$ implies the development of a robust ammonia carrier for using $SrCl_2$ in energy storage applications and NO_x abatement.

Ammonia as said before is a valuable chemical resource for use in industry as a fertilizer, refrigerant, and to refine petroleum. However, NH_3 is also a toxic gas that has a pungent odor and it has potentially harmful effects. Hence, NH_3 adsorption is of great importance for human health and the development of adsorbents for ammonia containment can exploit such expertise to its advantage. Ideal adsorbents possess high surface areas and small pore sizes. In recent years, the number of available nanoporous materials has increased substantially and emerged as a gas adsorbent alternative to the more common traditional. The highly regular pore structure and internal surface area of this structures make them attractive substrates that can be tailored for NH_3 adsorption.

There are two types of adsorption, physisorption and chemisorption. As the adsorption efficiency depends on the type of adsorbents, different kinds of low-cost adsorbents have been developed and tested to remove ammonium ions. There are kinds reported on the adsorption of ammonium ion by these low-cost adsorbents, e.g. polyvinyl alcohol (PVA) hydrogel, aerobic granular sludge, activated sludge and anammox granules, powders of leaves, stems or barks of some plants, municipal sludge. Furthermore, adsorbents should have good selectivity. That is to say, if adsorbents do not have high selectivity, the sorption capacity in real practice would always decrease. Likewise, since adsorption in some cases is reversible, adsorbents can be recovered by a reasonable desorption process, which makes the adsorption savvy in the applications.

For what we know a business developed a new product using strontium chloride, called AdAmmine for storing ammonia at low pressure, to use in SCR application. They guarantee that their protected material can likewise be produced using other AHMHs, however they have picked strontium chloride for large scale manufacturing. Prior organization research likewise considered involving the put away ammonium as a way to store engineered Ammonium fuel under the brand name HydrAmmine and the press name "hydrogen tablet", nonetheless, this new product has not been marketed. Their blueprint and materials are protected. Their initial investigations utilized magnesium chloride, and other AEMHs.

As we are moving out of from a world based on fossil fuel engines is important to address the fact that this type of adsorbents can be used to store the ammonia or applied in situations were ammonia can be recovered to promote a circular economy, as we know right now most of the removable ammonia is from waste water sources because it could reduce the amount of the latter produced by the energy-consuming HaberBosch process. Right now chemicals can be easily reclaimed from its aqueous solution via regenerated resins or biobased adsorbent. The tailoring of sorbent materials with respect to their surface charge and kinetics offers opportunities for efficient removal of charged compounds from solutions, for the Strontium chloride based structures, the application will be more challenging or nearly as the salts are soluble in water. For this other opportunities of gas ammonia emissions must be addressed and exploited as new source of ammonia for future use.

1.4 Strontium Chloride

As the main material of the study, some general information about strontium chloride must be displayed. As we can easily understand it is a salt of strontium and chloride and the formula is given as $SrCl_2$. Strontium, atomic number 38 in the periodic table, is a soft, silvery metal that burns in air and reacts with water, the discovery of this element is somewhat recent and it is dated at the end of the 18th century but it was only isolated in the early 19th century. Strontium has two oxidation states and it easily binds with Chlorine, as a salt in water forms neutral aqueous solutions and similarly to all the compounds of Sr it emits a bright red colour in a flame.

The crystalline solid of strontium chloride adopts a fluorite structure. In the vapour phase, the $SrCl_2$ molecule is represented as a non-linear having the Cl-Sr-Cl angle of approximately 130°.

Strontium chloride is prepared by treating either strontium carbonate or aqueous strontium hydroxide with hydrochloric acid. The chemical reaction for this can be given as follows:

$$Sr(OH)_2 + 2HCl \rightarrow SrCl_2 + 2H_2O$$

Crystallization from the cold aqueous solution produces the hexahydrate, $SrCl_2{\cdot}6\,H_2O$. Dehydration of this salt takes place in stages, commencing above 61 °C. Full dehydration takes place at 320 °C. Strontium chloride can be used as a red colouring agent in pyrotechnics. It also imparts a more intense red colour to the flames compared to most of the other alternatives. It can be employed in very small quantities in metallurgy and glass-making. The radioactive isotope, strontium-89, can be used for bone cancer treatment and is usually administered in the strontium chloride form. Seawater aquaria, need small amounts of strontium chloride, which can be consumed during the growth of particular plankton. It has been applied for dental care and as we will understand it can be used for ammonia storage.

From an atomic point of view the lattice parameter is in the order of 6.8 Armstrong and similar structure of CaF_2 and the unit cell is arranged where the bigger spheres are Cl ions and the smaller ones Strontium in a FCC motif (face centered cubic structure).

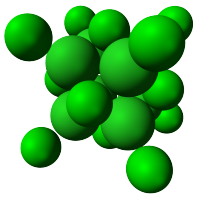

Figure 1.4: $SrCl_2$ unit cell

1.5 Sodium Bentonite

The other main raw material used as a sort of "matrix" to enable the possibility to print the structures made mainly of strontium chloride is sodium bentonite. Bentonite is a clay was formed in the Ordovician to Neogene periods, when volcanic ash was spread and in seas. As this started to dry up, the dissolved minerals, volcanic glass, started to concentrate which continually forced more and more chemicals and compounds to share less and less liquid space. This concentration made elements such as sodium freely available to react with the silicates, aluminum, and magnesium that constitute the backbone of the bentonite molecules. This sodium is what makes sodium bentonite the very different and remarkable

material that it is. Other forms of bentonite are also available, but these mostly have high concentrations of calcium, which give these bentonites different properties, substantially less swelling properties, sodium bentonite is what is used now to name the ore whose major constituent is the mineral, sodium montmorillonite.

Montmorillonites can be viewed as three layer structures where a central octahedral layer is in the middle of two tetrahedral layers. The sheet characteristic structure of this mineral is given by the bonding of the the shared oxide cations and anions of both type of layers, octahedral and tetrahedral, the oxides are aligned inward where they border with internal Al, Fe and Mg cations. From an overall charge stand point the montmorillonite have a total negative charge as the anions are in excess with respect to the cations giving the surface of the layers a negative charge, this characteristic gives the cations the ability to move freely between the layers as they are exchanged between the two. Bentonite is individuated by these three layers and characterized by 1nm thickness and 0.2-2microns in diameter, as the interspersing between the layers is affected by the presence and the amount of absorbed water bentonite powders are classified based on the predominate exchangeable cation, in nature the main ones are Sodium, Calcium and Magnesium. The Sodium ones show higher swelling properties as facilitates the absorption of water layers between the platelets. Calcium bentonites are generally low swelling.

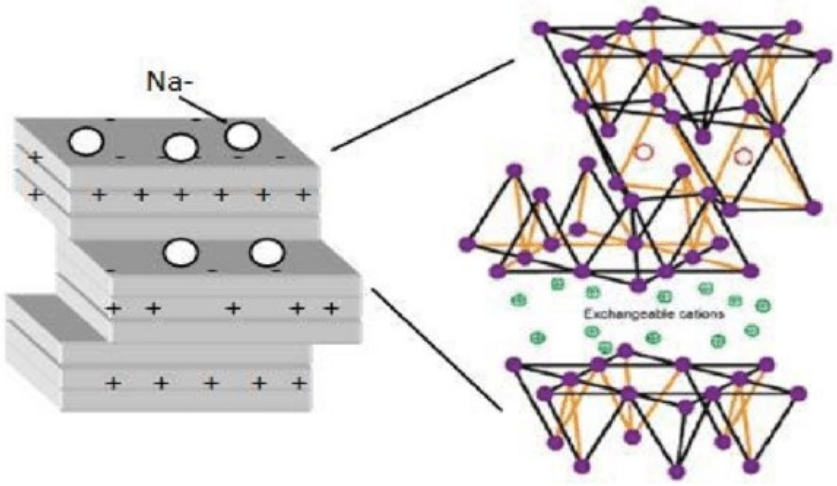

Figure 1.5: Crystalline structure of sodium bentonite with inter lamellar water layer

Viewed from above the bentonite platelet surface, oxygen atoms within the tetrahedral sheets are arranged in a hexagonal patter. Like matching pieces in a jigsaw puzzle, this pattern physically coincides with the pattern of the available hydrogen atoms in water molecules, and hydrogen bonding between the bentonites oxygen and the waters hydrogen atoms are possible.

1.6 Ammonia history and production

As the main focus of this work is ammonia a general introduction to what it is, what it is used for and how this chemical had a great impact in the human kind history must be done. Ammonia, chemical formula NH_3, from technical point of view, is a colorless poisonous gas at room temperature with a familiar noxious odor. In nature, it occurs primarily as a byproduct of anaerobic decay of plant and animal matter, as one of the basis of life on hearth it is must be noted that it is also has been detected in outer space. From a structural point of view the ammonia molecule is produced when three sp^3 hybrid orbitals of nitrogen and three s orbitals of hydrogens collide. A lone pair of electrons occupy the 4th sp^3 hybrid orbital of nitrogen this gives the ammonia molecule a trigonal pyramidal structure as a result. The H-N-H angle is 107.8°, while the N-H bond length is 101.7 pm. Due to lone pair-bond pair repulsion, which tends to push the N-H bond slightly inwards, the H-N-H bond angle is somewhat less than the tetrahedral angle of 109° 28 as ammonia contains hydrogen it is easily likable in liquid and solid.

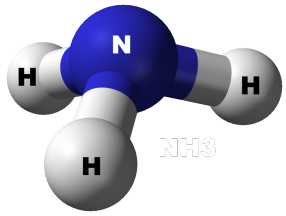

Figure 1.6: Ammonia strucutre

The breakthrough discovery of ammonia production was the stepping stone in human kind development, not only it overcame the food crisis of the early 20th but it gave birth to 5 billion people. As important as it is a digression of the history of the production of ammonia is introduced.

Ammonia was the subject of several scientific inquiries by the end of the eighteenth century, but up until then it had only been produced as a byproduct of other compounds. The substance had already been identified and was easily recognizable by its pungent smell, but it was only after the chemical composition was determined that the hypothesis of synthesis from the elements started to be considered. Ammonia was easily dissociable however, despite its apparently simple and analogue reaction of water formation, the synthesis of ammonia was wrongly conduced for more than a century and many erroneous reports of success stemming from improperly conducted experiments. The production of ammonia always seemed to have come from the influence of an additional factor, such in the atmosphere, causing people to wonder if the substance came from an entirely different type of reaction. A question made all the more mysterious by the extensive presence of ammonia in a natural environment, such as rotting organic matter.

Many started to question what took place in nature that could not be replicated in synthesis, and with modern knowledge we will now examine past experiments and consider why they failed in achieving their expected result. Many past attempts all seem to share two flaws: temperatures and pressures below the necessary thresholds. This brought many to believe that direct synthesis was effectively impossible, a notion plausible for the times, as it was under the assumptions that chemical reactions could only proceed in one direction. Before fundamental concepts of reversibility and equilibrium were known, the role of the catalyst could not be completely understood and the tangible absolute proof of the direct combination of hydrogen and nitrogen could not be found.

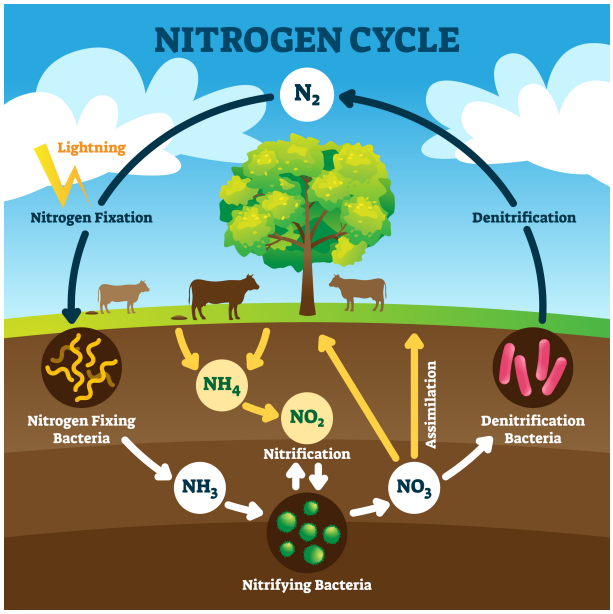

Figure 1.7: Nitrogen cycle

Not all experiments lacked in these two factors, however. Approaching mid century, higher temperatures, increased pressure and catalysts were all implemented in experimentation and by the end of the century elements of an emerging physical chemistry started being seen in experimental reports. At the time, many experiments revolved around the search for a reliable source of fixed nitrogen, due to increasingly desperate demand from politicians, economists and farmers. The scientific community shifted its focus then on the formation and dissociation of the ammonia molecule, the energetic nature and strength of its bond and the bonds of its constituents. The employment of fixed nitrogen in crop growth seemed to be the limiting factor according to the limited knowledge of the time. Some success was however seen as the usage of fertilizers, drainage systems and transport of biomass all opened the once closed nitrogen cycle. Intrigued by nature's biological ability to fix nitrogen or to do so through lightning strikes, scientists attempted to replicate these phenomena. While direct breeding and marketing of nitrobacteria ultimately failed,the natural multistep bacterial fixation was emulated in the cynamide and other processes entering the first quarter of the following century with low yields that could not be improved.

Direct synthesis of ammonia from the elements then gained further attention as the potential solution to the rising need of nitrogen fertilizer but remained, ultimately, unfeasible. The substance, despite being quickly dissociated catalytically, could not be produced in non irrisory amounts, since key physical insight was lacking at the time. During this time, a permanent solution to food production issues for the growing population became a pressing topic in official circles, as crops became much more strictly tied to specific areas and arable land was expected to keep decreasing in surface (as seen, for instance, in South America, where nitrogen supplies were on the verge of collapse). These sources of fixed nitrogen that could have alleviated hunger, were instead getting turned into a commodity used to better the lives of the wealthy as high-throughput farming was now dependent on this stock resource. Chemist William Crookes warned the British Association for the Advancement of Science in 1898 that civilized nations were on the verge of no longer being able to produce adequate quantities of foodstuffs. In his speech, he pointed to the fixation of atmospheric nitrogen as a potential answer to the issue of fixed nitrogen mass production. A speech that took place in a period of rising tensions throughout nations just before the Great War, when fixed nitrogen started being used for military explosives, mining and construction.

As Germany's chemical industry infrastructure became a reference point thanks to increased investments and improved infrastructure, further research in agricultural science showed the need for a synthetic source of fixed nitrogen. Natural sciences' further development, along with a new theoretical framework for chemical reaction, gave rise to the discipline of physical chemistry. William Crookes shone light on the key role of ammonia synthesis in the production of foodstuffs, highlighting the process as the potential solution to an increasingly grim humanitarian crisis and as a catalyst of economic development. In the years prior to Haber's studies, several scientists attempted synthetizing ammonia to no avail. One such scientist was WIlhelm Ostwald, a chemist that tackled this endeavour using a physicochemical approach. All of his experiments were carried on at atmospheric pressure with temperatures ranging between 250 and 300 C and employing a catalyst to raise the reaction rate. Current cognizance allows us to acknowledge Ostwald's methods as correct, if only in principle. His work was conducted lacking the experimental sensitivity necessary for the measurement of ammonia equilibrium and without taking into account the impact of the impure materials employed. What he considered a successfull synthesis of ammonia was only a contaminated experiment, since the ammonia he detected had been produced from the nitrogen contained in the iron catalyst he made use of. Following Ostwald's attempts, work on ammonia synthesis continued throughout the years until physical chemist Fritz Haber, using Ostwald's laboratory procedure, began experimenting using even higher temperatures and utilizing a variety of catalysts to achieve higher reaction rates. Haber was aware of the importance of measurement sensitivity and the usage of pure substances, as the notion of ammonia synthesis being a balancing act in principle was now much more widespread. During his testing, he observed that while high temperatures did indeed raise the reaction rate, going beyond a certain threshold rendered the catalyst inactive and caused the process of decomposition in ammonia to outpace its production. The Haber Bosh process brought several basic physicochemical principles into question but ultimately failed to bridge scientific understanding of the ammonia synthesis process with a cost effective process to produce it.

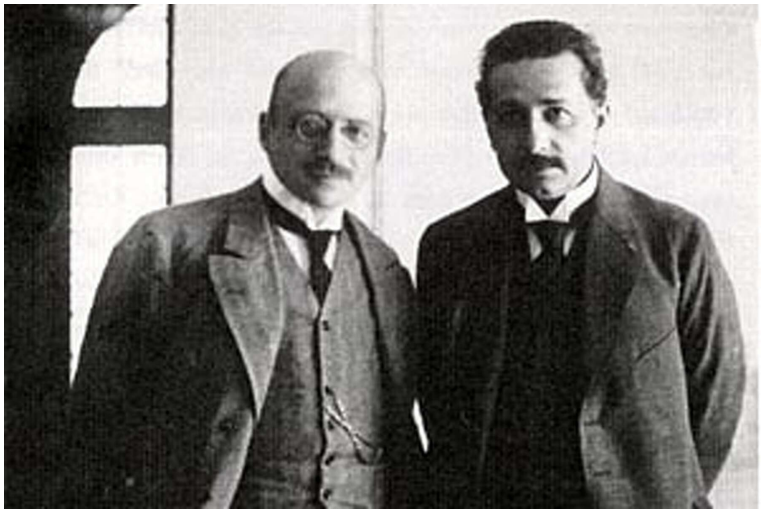

Figure 1.8: F.Haber and A.Einstein

Haber's breakthrough had consequences, which are still felt to this day, in the impact we have on the ecological equilibrium to feed the population and the manifacturing of explosives, which already started to show signs of their presence in the first half of the twentieth century, as facilities capable of mass producing nitrogen started spreading across the world. Although producing enough food to feed the world has become possible, the

former shortage of nitrogen has now become an excess that threatens water, air, and soil quality as well as entire ecosystems and biodiversity. The arable land is now saturated with nitrates, transported through runoff into environments, especially coastal regions and oceans, not intended to receive such chemical surpluses; the resulting imbalance impacts life in these areas, with phenomena such as hypoxia and eutrophication. It is in terrestrial and marine nitrogen cycles that the dynamic is most complex. In combination with natural conditions, it has contributed to changing quantities of biomass and species composition, effects felt not only the natural environment, but also in our own urban hubs and in fundamental changes in our social structure. The production of food has transformed, no longer the collection of the annual influx of solar energy, it now consumes other sources of power as well. We have advanced using technical progress and raw material from fossil fuels to boost a large input mechanism into the nitrogen cycle: fertilizer. Advances in modern mobility and transport have also resulted in new input mechanisms via the internal combustion engines producing ever increasing quantities of smog. The nitrogen cycle has not only been simply opened; man-made factors have bound the carbon and nitrogen cycles together in an unprecedented way. Hydrogen for the Haber-Bosch process is obtained by stripping it from hydrocarbons, and the residual nitrogen runoff affects the growth of biomass, linking it to levels of carbon, phosphorous, and other elements in several biogeochemical cycles. The effect of certain levels of greenhouse gases and the future of our climate have become difficult to assess,turning fixed nitrogen production into one of the most critical developments of our time. This is not to judge or to support the conclusion that all factors and consequences of synthetic fixed nitrogen are exclusively, inherently negative, but rather to remind us of the risks of continued excessive use. Natural environment has already been irreparably changed and often damaged from the output of the power-hungry HaberBosch process, which consumes 1-2 % of the world's total energy production. We need to find a way to meet our needs that doesn't only look to the short term. We are not yet in an irreversible situation and may still come full circle. We need to solve our problems not only using technology, but using an integrated that spans science, technology, industry, politics, with the help of public figures using their louder voices to shine light on this important topic. While the environmental impact caused by mass production of fixed nitrogen is undoubtedly vast, it was certainly not Haber's intention, and we should not blame him for it. Scientists do not, without further involvement, bare responsibility for the technological repercussions of their findings. However, moral questions do emerge regarding another aspect of ammonia synthesis. The production of fertilizer and the manufacture of explosives in Europe in the first decade of the twentieth century was heavily dependent on nitrate imports. As the First World War loomed, the possibility, and eventual actuality, of blocked maritime trading routes caused many in Germany to reconsider the general security of the country and led to massive investment in science and technology to obviate possible shortfalls. Beyond a synthetic source of nitrates, much of Haber's prewar work investigating gas reactions also learnt itself to another possibility for the war effort: the development of poison gas. This new type of weapon promised not only a solution to munitions shortages but also enabled a new strategy of warfare. After initial lackluster tests and attempted deployment in the beginning of 1915, chlorine gas was used at Ypres against French and British troops; the cloud of poisonous gas spread over the battle field, killing hundreds and injuring thousands . Within months Haber's research institute, already heavily involved in the German mobilization effort, grew rapidly in size and turned its attention entirely toward gas warfare, conducting research on mustard gas, phosgene, and other aggressive compounds as well as gas masks and respirators. Haber relished his role and influence as one of the earliest "intermediary experts" as the convergence of state, military, economy, and science began to transform research into something like what we recognize today as big science. The use of poisonous gas went against international law and declared as a war

crime, while Haber had insisted on the "humane" nature of chemical weapons to shorten the length of the war and limit the number of deaths. As Haber and his research institute kept developing tools of war, scientists determined methods for safely working with cyanides, one of which was called Zyklon A. Unforeseen by Haber, it's successor, Zyklon B, was later used against civilian populations. Research on poison gas, much like ammonia synthesis, shows the double-edged nature of scientific research, and in many ways Fritz Haber himself. Observing the entirety of these events, it becomes apparent that science and technological breakthroughs lead to changes in knowledge, means, and resources. Fundamental principles need not be completely understood at the outset for important results to be obtained. This is especially important if we consider the general public's expectations of science. The scientific endeavor is not an infallible activity of peerless precision, it is a continuous pursuit from fallible human beings, subjected to many of the same pitfalls that befall other disciplines.

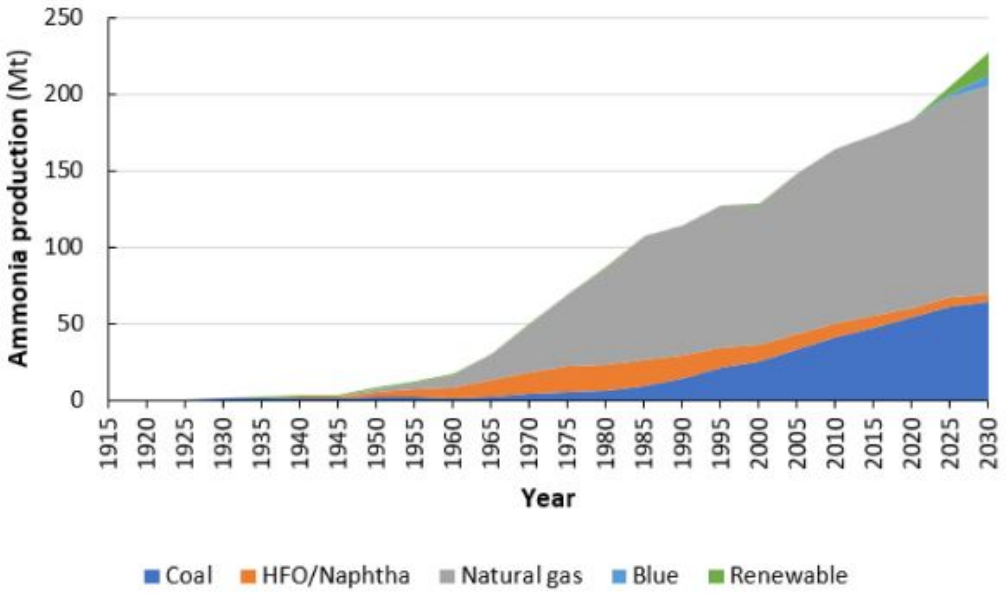

Figure 1.9: Yearly production of ammonia, source based

Currently ammonia is made from fossil fuel–derived hydrogen and is therefore not a "green" product, despite its widespread use in agriculture. But environmentally green ammonia may be on the horizon if the hydrogen is made by other means, such as wind or solar powered electrolysis of water. Ammonia production has increased steadily since 1946, and fast forward to the current era only in 2020, the worldwide ammonia production capacity was 224 million tonnes (Mt). Actual production was 187 Mt and it ranks ninth among chemicals produced globally. Most ammonia production 85% is used directly or indirectly in agriculture. Chemical fertilizers made from ammonia include urea, ammonium phosphate, ammonium nitrate, and other nitrates. Other important chemicals produced from ammonia include nitric acid, hydrazine, cyanides, and amino acids. Probably the most familiar household use of ammonia is in glass cleaners.

Even the positive application of ammonia synthesis has repercussions. Haber could not have foreseen “the cascade of environmental changes", including the increase in water and air pollution, the perturbation of greenhouse-gas levels and the loss of biodiversity that was the result from the colossal increase in ammonia production and use that was to ensue. However, nitrogen fertilization will not be abandoned any time soon. The world’s population is expected to grow to 9 billion by 2042, and further increase our dependence on nitrogen fertilizers. A number of different scenarios for future nitrogen fertilizer use and the challenges likely to be faced. For promoting a circular economy investment must be done in the field of sorbents for the removal of contaminant ammonia and the reuse of it, some studies were done using polymer-zeolite composites and geopolymers [9][10]. Maybe this could be the route the reduce the environmental impact of the production of ammonia.

1.7 Additive manufacturing

Additive manufacturing is the formalized term for what used to be called rapid prototyping and what is popularly called now 3D Printing. In the late 1980s, technology development caught up with the idea of manufacturing products with an additive approach, rather than through traditional subtractive or forming approaches, emphasizing a new view, based on fastness. Among other things, the idea was to open up a new design space, where e.g. new geometries or material compositions could be explored. Referred to in short as AM, the basic principle of this technology is that a model, initially generated using a three-dimensional Computer-Aided Design (3D CAD) system, by means of different software’s, can be fabricated directly without the need for process planning. Although this is not in reality as simple as it first sounds, AM technology certainly significantly simplifies the process of producing complex 3D objects directly from CAD data, but introduces a different type of challenges. Other manufacturing processes require a careful and detailed analysis of the part geometry to determine things like the order in which different features can be fabricated, what tools and processes must be used, and what additional fixtures may be required to complete the part. In contrast, AM needs only some basic dimensional details and a small amount of understanding as to how the AM machine works and the materials that are used to build the part.

The key to how AM works and its power is that parts are made by adding material in layers; obviously as the machine tries to produce the peace, each layer must have a finite thickness to it and so the resulting part will be an approximation of the original data. The thinner each layer is, higher resolution will be to the original image produced in the software. As we understand the approach of AM is totally different from an industrial view point, as we don’t need to shape the material according to an image but is the image that shapes the material accordingly, this makes the prosses “fast” by reducing process steps as we create a near net shape component, by selectively adding the material where it is needed. By doing this near net shape components can be achieved with little material waste whereas conventional manufacturing methods produce considerably more waste material. All commercialized AM machines to date use a layer-based approach, and the major ways that they differ are in the materials that can be used, how the layers are created, and how the layers are bonded to each other. Such differences will determine factors like the accuracy of the final part plus its material properties and mechanical properties. They will also determine factors like how quickly the part can be made, how much post-processing is required, the size of the AM machine used, and the overall cost of the machine and process. AM technology was originally developed around polymeric materials, waxes, and paper laminates. Subsequently, there has been introduction of composites, metals, and ceramics. However, much work still remains to be done before AM is a real contender of replacing conventional manufacturing

methods. In industrial applications AM is at present state regarded as a complement to conventional manufacturing methods with the potential to add value to the manufactured components. One of the biggest challenges of any AM method is the relatively low building rate compared to the conventional production methods. This limits the applications to which AM is economical viable to small complex parts, repairing and reinforcing, small series production, and production of components that virtually cannot be manufactured by any other method e.g. honeycomb structures for filtration applications.

1.8 Direct ink writing

One of the most broadly spread and feasible technique is the extrusion-based AM by means of direct ink writing. In all material extrusion-based technologies the material contained in a reservoir is forced out through a nozzle when pressure is applied. If the pressure remains constant, then the resulting extruded material flow at a constant rate and will remain a constant cross-sectional diameter. This diameter will remain constant if the travel of the nozzle across a depositing surface is also kept at a constant speed that corresponds to the flow rate. The material that is being extruded must be in a semisolid state when it comes out of the nozzle and fully solidify while remaining in that shape. Furthermore, the material must bond to material that has already been extruded so that a solid structure can result. There are two primary approaches when using an extrusion process. The most commonly used approach is to use temperature as a way of controlling the material state. An alternative approach is to use a physio-chemical change to cause solidification. In such cases, a curing agent, residual solvent, reaction with air, or simply drying of a “wet” material permits bonding to occur. Parts may therefore cure or dry out to become fully stable. This approach can be utilized with paste materials. Then the printing process can be controlled by means of tailoring the parameters of the printer, such as pressure and speed.

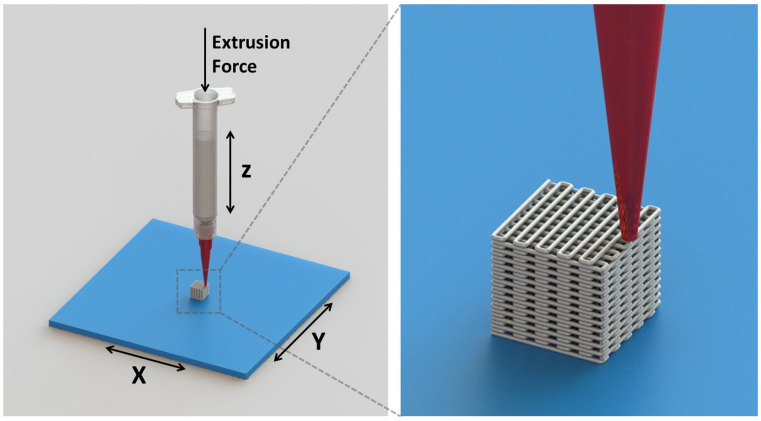

Figure 1.10: Schematics of how the 3D printing process by DIW works

1.9 Adsorption-Absorption-Sorption

Adsorption is now getting recognized as an effective and economical method for ammonium removal. In general, "adsorption is defined as the enrichment of molecules, atoms or ions in the vicinity of an interface. In the case of gas/solid systems, adsorption takes place in the vicinity of the solid surface and outside the solid structure. The material in the adsorbed state is known as the adsorbate, while the adsorptive is the same component in the fluid phase and adsorption space is the space occupied by the adsorbate" (IUPAC technology

report) [11]. In fields like heterogeneous catalysis and sorption (sorbents for gases, metals, organic matter), we are interested in the surface of the adsorbent or catalyst, and less in the bulk of the material. For applications in heterogeneouscatalysis or adsorption, it is important that the material has a high specific surface area (expressed as m^2g^1), and preferably pores of uniform size with a high pore volume (expressed as mlg^1). The word specific in the surface area means the value is normalized to 1g of material. Most materials are irregular in shape, and indirect methods are required to assess the surface area. The most used technique is the adsorption of a well-known gas. If the mean cross-sectional area (i.e. the amount of space that the adsorbed molecule occupies on the surface of the solid material, expressed in nm^2) of the gas molecule is known, and if the amount of gas required to form exactly one adsorbed monolayer on the surface can be determined, the surface area can be easily calculated (BET analysis).

Depending on the strength of the interaction, all adsorption processes can be divided into two categories of chemical and physical adsorption, chemisorption and physisorption. When talking about this process we need to define the adsorpitive, that is the adsorbable gas and the adsorbant, the substrate were the adsorption happens, when the two come in contact two type of interaction could happen, mainly two physisorption and chemysirption based on the froce of the bond. In physisorption a physical bond is generated, and is characterized by Vander Waals forces. In chemisorption the intermolecucalr forces are stronger and involve chemical bond.

When the molecules of the adsorptive comes into contact with the surface layer and enter the the bulk solid, the term absorption is used, instead when the molecules are debonded from the strucutre the term desorption is used. It is sometimes difficult or impossible to distinguish between adsorption and absorption: it is then convenient to use the wider term sorption which embraces both phenomena, and to use the derived terms sorbent, sorbate and sorptive.

Examples of chemisorption include the modification of the surface of supports by a surface reaction with other chemicals. For heavy metals the adsorption is prompt by Van der Waals bonds (physisorption), due to electrostatic interactions or ionic exchange properties of the surface, while for light metals or molecules the bonding might be related to chemical interactions as (chemisorption). Extensive studies were made on the characterization and adsorption performance of different kind of material based porous structures. The objecive is to have very high removal rates of the target species and usually they can be modified to enhance the characteristics, reusability.

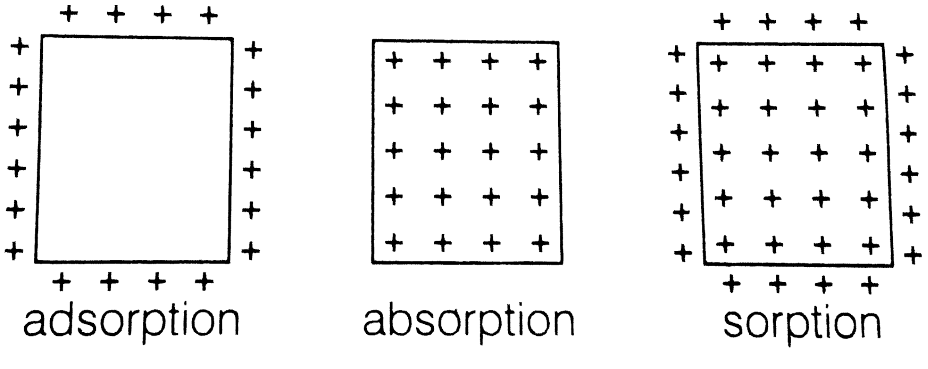

Figure 1.11: Visualisation of the adsorptio-absorptio-sorption process

The properties of a system most significant for this type of sorption process are those related to the surface at which accumulation occurs. Driving forces for attainment of chemical equilibrium in homogeneous phases relate to reduction of the free energies of bulk systems,

whereas the driving force for a surface reaction is a reduction in surface energy. One common manifestation of surface energy occurs when a drop of liquid placed on a flat solid surface resists spreading, and attempts to gain or retain a nearly spherical shape. The liquid in this case is attempting to minimize its free surface energy. This phenomenon, the development of a tension at the surface, results from attractive forces between molecules of the solid plate or molecules of liquid within the drop. Because molecules of the liquid are attracted more strongly to one another by cohesion forces than they are to molecules of the solid plate at the liquid-solid interface, molecules of liquid at the surface will be pulled mainly toward the interior of the drop. The same effect applies to the air-liquid interface, which thus tends to decrease its exposed surface as a result of the surface tension developed by the molecular cohesion forces. A pure liquid always tends to reduce its free surface energy through the action of surface tension. From a molecular point of view, enlarging a surface requires the breaking of bonds between surface molecules of the liquid phase, and the forming of bonds between these molecules and those of adjacent phases. A wide variety of soluble substances can alter the surface tension of a liquid. Surfactants, for example, lower the surface tension of water and cause it to spread on a solid surface, resulting in a wetting of that surface. Such substances are therefore termed wetting agents. If a surface active solute is present in a liquid system, a decrease in the surface tension of that liquid will occur upon movement of the substance to the surface. Stated another way, any solute known to lower the surface tension of a liquid will migrate to, and adsorb at, the interface of that liquid with some other phase. It is possible to define rigorous relationships for conditions in which equilibrium inter-facial tension is reduced with increasing concentration of a solute sorbed at an interface, but for this purpose they are not of interesting.

1.10 Porous materials

Porous materials are materials that contain voids, channels, holes, or basically pores. This type of material has always attracted a lot of attention as the presence of pores means that the material possesses an internal surface area of interest for all type of applications. Porous solids can be arranged in three main categories, depending on their pore size (diameter, d), according to IUPAC:

- micro- for pore sizes of less than 2 nm:
- meso- for pore sizes of 2–50 nm:
- macroporous for pore sizes over 50 nm;

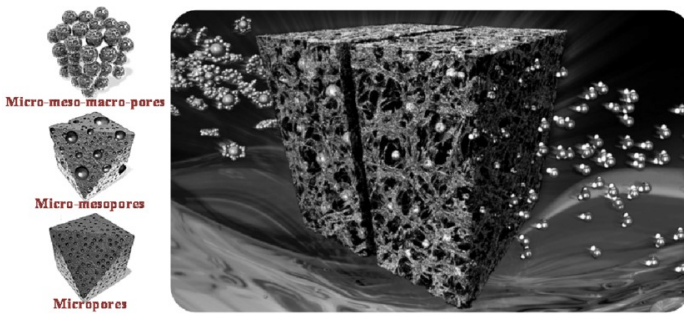

Figure 1.12: Representation of different types of porous materials

Nowadays, many porous materials are made in the laboratory and can even be produced on a large industrial scale. However, many porous materials are not an in invention but naturally occurring, like the wings of butterflies are not only colorful and useful to fly, but they are also porous. The scales on the butterfly wings are made of micro and nano porous structure achieving particular interaction to the light giving the wings their special and vibrant coloring. An everyday example of porous material is paper. Paper is the most ancient of all humanity artificially made porous products, the Chinese Chronicle reported that paper was invented in 105 AD by Tsai Lun. However, in 1957, in the Baotsya Cave in northern China's Shansi Province, a tomb was discovered where scraps of paper sheets were found. And after 150 years, via prisoners of war it came to be known by the Arabs. In the sixth to eighth centuries, paper production was carried out in Central Asia, Korea, Japan, and other Asian countries. In the eleventh to twelfth centuries, paper appeared in Europe, where it replaced animal parchment until nowadays were milion of tons are produced every year. The Porosity inside paper directly affects the absorbency of paper, that is, its ability to receive the ink and may well serve to characterize the structure of paper, paper can be macro or microporous and based on its structure different sorption characteristics will result. Other technical porous materials are developed like Porous metals are a relatively new class of engineering materials that can serve functional and structural purposes they have undergone rapid development over the last thirty years. These lightweight materials not only have the typical characteristics of metals (weldability, electrical conductivity, and ductibility), but also possess other useful characteristics, such as low bulk density, great specific surface area, low thermal conductivity, good penetrability, energy management, mechanical damping, vibration suppression, sound absorption, noise attenuation, and electromagnetic shielding. Consequently, these materials have increasing applications, and have emerged as a focus of great attention in the international material field.

Porous ceramic materials consist of at least two phases: a ceramic (solid) phase, and the mostly gas-filled porous phase. The gas content of the pores usually adjusts itself to the environment as an exchange of gas with the environment is possible through pore channels. Closed pores can contain a gas composition that is independent of the environment. The ceramic (matrix) material can either be single phase or, as is often the case, multi-phase (e.g. one more crystalline phases and a glass phase). As for the structure it possible to have honey comb and ceramic foams. When specifying the porosity, a distinction needs to be made between open (accessible from the outside) porosity and closed porosity. Open porosity can be further classified into open dead-end pores and open pore channels. Depending on the particular application, either a more open porosity (e.g. a filter element that needs to be permeable) or a closed porosity (e.g. a thermal insulator) may be desired. The sum of the open and closed porosity is referred to as the total porosity. If the fractional porosity of a material is relatively low, then the closed porosity will dominate; as the fractional porosity increases, the open porosity level increases. A literature review on the analysis of numerous materials (UN, porous metals, ZrO2, graphite foam, MgO granulates, stainless steel and UO2) has been carried out by Schulz. Besides specifying the type and degree of porosity, it also important to describe the size distribution of pores when describing a porous material. Several properties of the matrix material are not influenced by porosity and are therefore also applicable to the porous material (e.g. coefficient of thermal expansion), however most properties are dependent on the total porosity and therefore need to be redetermined for the porous material (e.g. mechanical strength, electrical properties, etc.).

CHAPTER 2

Materials and methods

This chapter, lists all the main raw materials, instruments and briefly described the methods used during experimentation. The objective was to produce by DIW a porous structure made of bentonite and strontium chloride at different concentrations. Many methods can be employed, but extrusion based ceramic additive manufacturing generally adheres to a process flow common to all techniques. This process flow involves three main operations: slurry preparation, printing, and possible thermal treatment. The details of each process varied significantly between methods, but the end result accomplished the same goal. Before, during, and after these processes, measurements and observations were made to characterize both the material system and the process itself.

2.1 Materials

- Strontium Chloride $SrCl_2$(Sigma-Aldrich), white pale crystals ;
- Sodium Bentonite, brown-green dust;
- Distilled water.

Chemicals	MW(g/mol)	Density(g/mL)	Formula
Strontium Chloride	158.83	3.05	$SrCl_2$
Sodium-Bentonite	266	1.6-1.8	$Al_2H_2Na_2O_{13}Si_4$
Distilled H2O	18.02	1	H_2O

Table 2.1

The main constituent of the slurry is a physical mixture of $SrCl_2$ and bentonite, to which distilled water is then added. Batches of powder with different fractions of the two starting materials were prepared, as shown in the following table:

Strontium Chloride(%)	Sodium-Betonite (%)
70	30
80	20
60	40

Table 2.2

For the preparation of each composition a weight of 50 g was chosen and the amount of raw material, based on the mass fraction, was measured on an analytical scale and placed into an agate ball milling jar. The material was milled at 360 rpm for 15 rounds (15 minutes active and 5 pause). The dust obtained was sifted at a dimension lower than 63 microns and stored in a plastic container for future use.

$SrCl_2$ at room temperature tends to absorb water and became hexahydrate, if we assume this happens even for the concentrations above, some calculations must be carried out to understand the real percentage of $SrCl_2$ in the mixture. Assuming a starting mass of 50 g, we need to calculate first the moles of $SrCl_2$ and assuming that it is all present in hexahydrate form we can find the mass of the hydrate salt and find the final percentage of bentonite and $SrCl_2$. The table Tab 2.3 shows the actual mass fraction of $SrCl_2$ in the composite assuming that 100% hexahydrate is used in the formulation and that all water present in the slurry evaporates during drying.

Strontium Chloride hexahydrate(%)	Strontium Chloride (%)
70	58.33
80	70.48
60	47.24

Table 2.3

2.2 Ink preparation and printing

The DIW deposition process can be divided into three steps: (1) the flow of the ink through the syringe barrel and printing nozzle; (2) the ejection of the ink from the nozzle, so shear-thinning behaviour and (3) the deposition of the ink onto the underlaying printed layers. During each one of these fundamental steps, the ink should meet specific requirements to be printable. It has often been highlighted that the concept of printability is not universal, and it is strictly related to the use and application of the printed object. As a very general definition, an ink is considered printable if it can be extruded through a selected nozzle in the form of a continuous filament, able to build structures that accurately replicate the digital model. The morphology of the printed structure should be retained after deposition, drying and post-processing.

In this application the ink was prepared by weighting different quantities of powder and mixing with water, the ratio of the two varied according to the formulation as reported in the Tab. 2.4. The powder and water were placed into a glass vial and then homogenized on a high-energy planetary mixer for about 15 minutes in rounds of 5. Particular attention was placed on keeping the temperature of the vial low, to avoid re-crystallization and ensure good rheology: thus, cold water was used and after each round the vial was placed in a freezer. Before loading the ink into the syringe a cycle of 15 minutes of sonication was performed. The ink (6 grams) was then loaded into a small syringe (max weight 8 grams) and a nozzle of 0,41 mm diameter was used. The scaffolds were printed on Teflon sheets to help the removal. The printed samples were then placed in an oven set at 40°C for a few days for the drying stage.

Strontium Chloride(%)-Sodium-Betonite (%)	Mass ratio with water
70-30	1.82
80-20	1.71
60-40	1.71

Table 2.4

Before choosing the optimised route for the ink preparation, different strategies were tried: first the ink was mixed using an electronic stirrer, but the low amount of material made the approach unfeasible so the planetary mixer was chosen instead; for the same reason a screw extruder was not used during the printing step. The compositions were chosen among many attempts mainly for the possibility to produce easily an ink that could perform without major problems related to the rheology. The ink was optimized to print a very high speed and pressure, so it was necessary to ensure a good fluidity to it; a slower approach was also attempted but with poorer results.

2.2.1 Porous structure Design

The design flexibility of Additive Manufacturing processes allow for the production of porous monoliths with highly controllable geometric properties. Porosity as mentioned before is desired in a broad range of materials for different applications like catalytic supports, lightweight structures, and biomedical scaffolds. For this study a single design was used for all the the different compositions. After loading the syringe, the pressure tube was applied to check if the ink was flow consistently out of the nozzle and find the right working pressure (typically 4-5 bar). The syringe was then fixed to the 3D printer. During the extrusion different parameters were changed to according to the rheological characteristics of the ink: as a rule of thumb, when the ink was too fluid the speed of the printer was increased and vice-versa. As shown in Fig 2.1 the scaffolds were small so the printing process for a single sample was in the order of 2-3 minutes

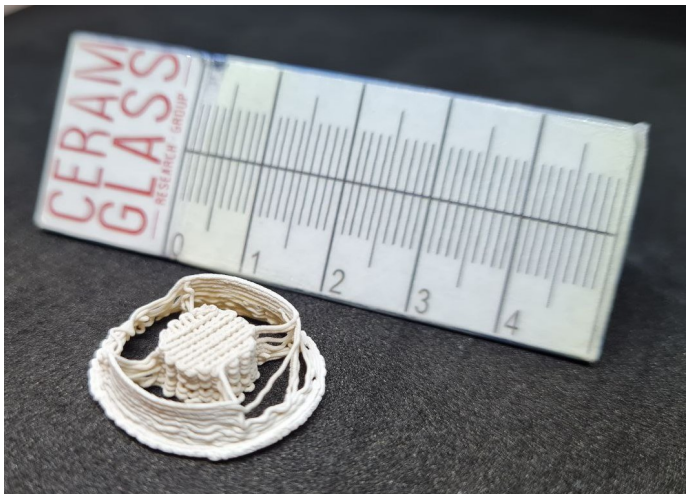

Figure 2.1: Printed Strontium chloride monoliths

2.3 Thermal treatment

The thermal treatment was performed in atmosphere, under pressureless conditions. For this research, the thermal treatment was performed in a high temperature muffle furnace. Generally, when trying to create fully dense materials, bulk, or volume, diffusion is the dominant form of mass transport, generating the most densification. Volume diffusion dominates after the temperature surpasses approximately half of the material melting temperature. For creating a lesser dense structure but with enhanced physical properties, the thermal treatment schedules consist of a fast heating ramp to a temperature near 0.90 Tm, a holding time, then a relatively slow cooling to avoid part failure by thermal shock. The thermal treatment was only performed to the 70% composition, as the structure obtained after the process hinders the absorbance capabilities of the structure. The heating was performed in two steps to avoid possible breakage due to thermal stresses, a first slow ramp to 350°C at 1°C/min (as this is the region where $SrCl_2$ hydrates revert back to the anhydrous form) followed by a faster heating to 800°C at 5°C/min, 2h dwell and eventually slow cooling with the furnace off until room temperature. The micro-structure obtained was evidently different from the one of the untreated specimen as shown by the SEM images in Chap. 3.

2.4 Mechanical properties

For ceramics to be used reliably as structural engineering materials, an understanding of the mechanical properties is necessary. A comparison of these properties with values gives insight into quality and potential applications. The mechanical compressive properties of the porous structures were evaluated using a press for uniaxial compression tests. Fracture of brittle materials (e.g. ceramics) usually initiates from flaws, which are distributed in the material. The strength of the specimen depends on the size of the major flaws, which varies between specimens. Therefore the strength of brittle materials has to be described by a statistical probability function. The Weibull distribution function is the basis of the state of the art in mechanical design procedure of ceramic components. It should be noted that in almost every experimental study on fracture statistics of ceramics it is claimed that the data are Weibull distributed. The fundamental assumption is the weakest link hypothesis, i.e. the specimen fails, if its weakest volume element fails. It follows from the experiments that the probability of failure increases with load amplitude and with size of the specimens. The first observation is trivial. The second observation follows from the fact that it is more likely to find a major flaw in a large specimen than in a small one. Therefore the mean strength of a set of large specimens is smaller than the mean strength of a set of small specimens. This size effect on strength is the most prominent and relevant consequence of the statistical behaviour of strength in brittle materials. The Weibull distribution is a continuous probability density distribution widely used for analysis of reliability over time or failure rate of a component or material. By studying the failure results of a large number of samples, can be composed into a histogram in which the number of samples have broken in defined intervals of effort, such histogram can be described analytically by a function f, were σ is the stress applied and sigma zero the scale parameter, specific of the distribution.

The *f* equation is defined by the parameter m and sigma zero, m is the shape parameter and for positive values the failure rate increases with applied stress and a more narrow range for the fail stress, meaning a less "static failure", while for decreasing vice versa. Both parameters can be obtained by expressing the equation for the survival probability in its linear form::

$$f(\frac{\sigma}{\sigma_0}) = \frac{m}{\sigma_0}(\frac{\sigma}{\sigma_0})^{m-1} exp(-(\frac{\sigma}{\sigma_0})^m)$$

$$lnln\frac{1}{S} = mln\frac{\sigma}{\sigma_0} = mln\sigma - mln\sigma_0$$

plotting *ln ln (1 / S)* vs. *ln* σ it is possible to derive the values of m and from the experimental data.

Then to determine the values of m and sigma zero it is necessary to draw the Weibull diagram for each batch. To do this, the fracture stress values of the N samples are ordered from the smallest to the largest, remembering that the survival probability of the first sample, the one that failed with the smallest load, is obviously the highest. Moving along the list of samples, the probability of survival decreases and eventually becomes minimum at the *N-th* sample. The approximate relation of the probability of survival *Sj* of the *j-th* sample used in this study, is shown below together for the equation for calculate the σj of each sample analyzed:

$$S_j = 1 - \frac{j - 0.5}{N}$$

$$\sigma = \frac{F}{A}$$

All the the dimensional characteristics and the data for the Weibull analysis are collected in APpendix A (pag.57). With the values of lnσ and ln(ln(1 / S)) it is possible to proceed with a linear regression, this will give back a straight line in the form y = mx + c which will have the coefficient m as slope. The scale factor σ_0 was derived using the equation:

$$\sigma_0 = exp(-(\frac{intercept}{m}))$$

Before the compression test each sample was measured and weighed, than placed between the two plates of the mechanical test machine and subjected to compression at 0.5 mm/min until failure.

2.5 Brunauer, Emmett and Teller theory (BET)

For a long time, measuring the surface are of solids, particularly those with porous or otherwise complicated surface geometries, was not readily possible. However, this changed in 1938 with the introduction of the BET (Brunauer, Emmett and Teller) theory, is commonly used to evaluate the gas adsorption data and generate a specific surface area result expressed in units of area per mass of sample (m^2/g). Adsorption is defined by IUPAC as an increase in the concentration of a substance at an interface, in the case of the BET theory This kind of adsorption can be divided into two types, chemisorption and physisorption. Physisorption is reversible adsorption which is caused by van der Waals forces, where there is no (signifcant) changes in the electronic structure of the adsorbed species. In simpler terms, there are no bonds formed or broken when the gas is adsorbed at the solid surface. In contrast, in chemisorption a chemical reaction happens between the adsorbed species and the solid and

new bonds are formed. Physisorption is the physical phenomena on which BET surface analysis is based, and it is usually visualized in a plot known as an isotherm. The data for an isotherm is collected by measuring the equilibrium adsorption of the gas on the solid at different gas partial pressures at a constant temperature. The plot has the gas partial pressure on the x-axis and the amount adsorbed on the y-axis. The isotherm shows both the volume adsorbed at adsorption and at desorption, measured by first increasing the partial pressure of the gas, and then decreasing it back to high vacuum. Physisorption is a reversible phenomenon, however in the presence of mesopores (2nm < d < 50nm) gas entering the pores is condensed in them, due to the small pores changing the vapor pressure of the gas (capillary condensation).

The technique is referenced by several standard organizations such as ISO, USP and ASTM and is widely used for most materials. Prior to analysis, the sample must be preconditioned to remove physically bonded impurities from the surface of the powder in a process called degassing or outgassing. This is typically accomplished by applying elevated temperature to the sample in conjunction with vacuum or continuously flowing inert gas. This process must be carefully controlled and monitored in order to generate the most accurate and repeatable results. The specific surface area of a material is then determined by the physical adsorption of a gas (typically nitrogen, krypton, or argon) onto the surface of the sample at cryogenic temperatures (typically liquid nitrogen or liquid argon temperatures). The choice of gas to be used is dependent on the expected surface area and the properties of the sample. Once the amount of adsorbate gas has been measured (either by a volumetric or continuous flow technique), calculations which assume a monomolecular layer of the known gas are applied. BET surface area analysis must be done in the linear region of the BET plot, which could be systematically evaluated using the Rouquerol transform. This value is termed volume-specific surface area (VSSA) and is obtained by multiplying the BET surface area with the density of the material. Determining the surface area of a solid material is vitally important for many applications. The most commonly used model for surface analysis and follows the next equations, where P is the equilibrium pressure, P_0 the saturation pressure, n the adsorbed gas quantity (e.g., in volume units, at standard pressure (STP)), n_m the monolayer adsorbed gas quantity, and c the BET constant. By plotting the $P/n(P_0\ P)$ vs. P/P_0 at $0.05 < P/P_0 < 0.30$ (known as the BET plot), the n_m and c can be calculated through the slope and y-intercept. With that, the BET specific surface area can be obtained according to the second equation, where N_A is the Avogadro constant ($N_A\ \ 6.023 \times 1023 mol^{-1}$), s the adsorption cross-section of the adsorbate, V the molar volume of the adsorbate ($0.0224 m^3 mol^{-1}$ STP), and M the mass of the sorbent.

$$\frac{P}{n(P_0 - P)} = \frac{c-1}{n_m c}\frac{P}{P_0} + \frac{1}{n_m c}$$

$$S_{(BET)} = \frac{n_m N_A s}{VM}$$

The gas adsorption isotherms can reveal the pore type, as mentioned, according to the IUPAC, physisorption isotherms are classified into six types, as shown in Fig. 2.6.

Based on the shape of the isotherm different pore size can be matched.

- type I depicts monolayer adsorption. The characterization of microporous materials, those with pore diameters less than 2 nm, gives this type of isotherm. ;
- A type II isotherm is the most common isotherm obtained when using the BET technique. At very low pressures, the micropores fill with nitrogen gas. At the knee, monolayer formation is beginning and multilayer formation occurs at medium pressure. At the higher pressures, capillary condensation occurs.;

- A type III isotherm shows the formation of a multilayer. Because there is no asymptote in the curve, no monolayer is formed and BET is not applicable.;
- Type IV isotherms occur with capillary condensation. Gases condense in the tiny capillary pores of the solid at pressures below the saturation pressure of the gas. At the lower pressure regions, it shows the formation of a monolayer followed by a formation of multilayers. BET surface area characterization of mesoporous materials, which are materials with pore diameters between 2 - 50 nm, gives this type of isotherm.
- Type V isotherms are very similar to type IV isotherms and are not applicable to BET.

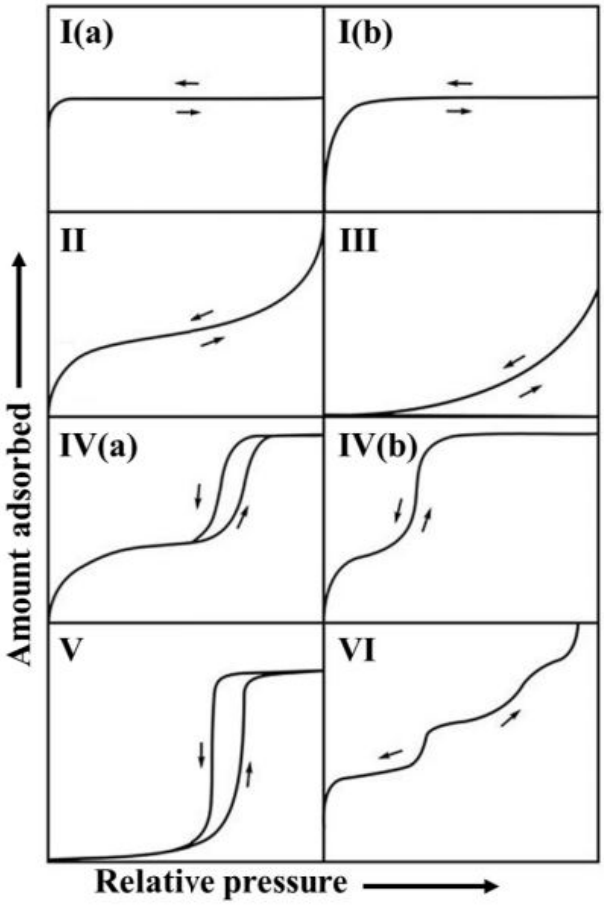

Figure 2.2: Isotherm shapes

The BET analysis returned different isotherm patterns for each composition, as said before there are many different shapes of hysteresis and even different loops have been reported, but the main types are shown in Fig. 2.2. Types H1, H2(a), H3 and H4 were identified in the original IUPAC classification of 1985, which is now extended in the light of more recent findings. Each of these six characteristic types is fairly closely related to particular features of the pore structure and underlying adsorption mechanism and the hysteresis is usually attributed to the thermodynamic or network effects or the combination of these two effects.

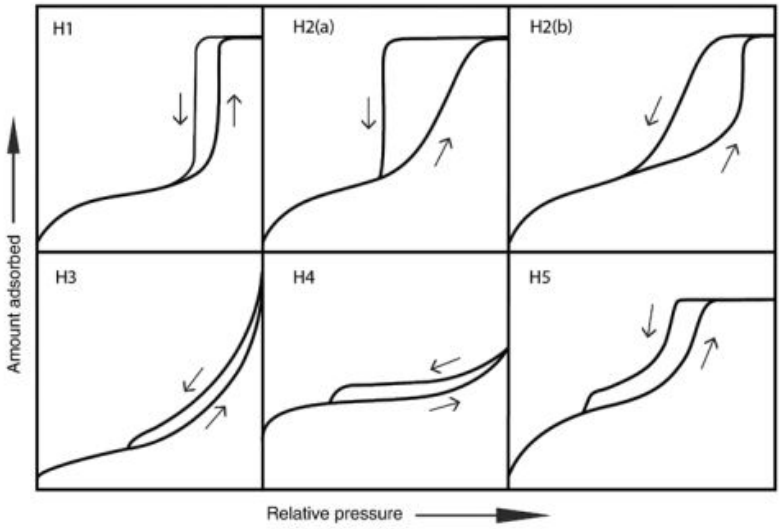

Figure 2.3: Types H1, H2(a), H3, H4cand H5 isotherms

The sorption isotherm that has a hysteresis are identified by a letter H followed by a number Fig 2.3. "The Type H1 loop is found in materials which exhibit a narrow range of uniform mesopores. Hysteresis loops of Type H2 are given by more complex pore structures in which network effects are important. The Type H2(b) loop is also associated with pore blocking, but the size distribution of neck widths is now much larger. There are two distinctive features of the Type H3 loop: (i) the adsorption branch resembles a Type II isotherm (ii) the lower limit of the desorption branch is normally located at the cavitation-induced p/P_0. Loops of this type are given by non-rigid aggregates of plate-like particles, but also if the pore network consists of macropores which are not completely filled with pore condensate. The H4 loop is somewhat similar, but the adsorption branch is now a composite of Types I and II, the more pronounced uptake at low p/P_0 being associated with the filling of micropores. Although the Type H5 loop is unusual, it has a distinctive form associated with certain pore structures containing both open and partially blocked mesopores. As already indicated, the common feature of H3, H4 and H5 loops is the sharp step-down of the desorption branch. Generally, this is located in a narrow range of p/P_0 for the particular adsorptive and temperature" [11].

For the analysis the samples were degassed at 150° in vacuum for 16 h prior to analysis, N_2 at 77 K was used as adsorbate.

2.6 X-ray diffraction XRD

X-ray diffraction (XRD) is a non-destructive technique for analyzing the structure of materials, primarily at the atomic or molecular level. It works best for materials that are crystalline or partially crystalline (i.e., that have periodic structural order) but is also used to study non-crystalline materials. Crystalline structures are defined as any structure of ions, atoms, or molecules that form in an ordered, three-dimensional arrangement. As the ions, atoms, or molecules are regularly spaced, they act as a three-dimensional grating.

XRD relies on the fact that X-rays are a form of light, with wavelengths on the order of nanometers. When X-rays scatter from a substance with structure at that length scale, interference can take place, resulting in a pattern of higher and lower intensities. This is qualitatively similar to the colorful patterns produced by soap bubbles, in which different colors are viewed in different directions. This pattern is determined by Braggs law, which

is defined as $n\lambda = 2d\sin\vartheta$, where n is the order of diffraction, λ is the wavelength of the incident X-rays, d is the interplanar spacing of the crystal and ϑ is the angle of incidence. This law relates wavelength to diffraction angle and the atomic spacing of the lattice within a crystalline sample (known as d-spacing). By using a fixed wavelength (i.e. monochromatic x-ray) the d-spacing can be determined for a specific angle. Rotating either the sample or the detector through a full range of angles allows for the full profile of the material to be measured.

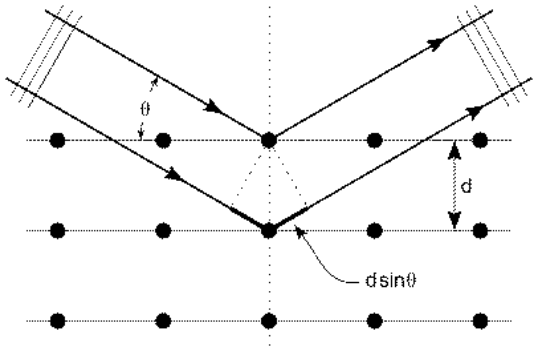

Figure 2.4: Bragg laws schematics

The instrument can be divided in different parts: x-ray source, x-ray gun necessary to focus the x-ray beam in the sample section and the detector that can move to collect all the scattered beams. The instrument produces a pattern of diffracted intensity vs angle, characterized by the presence of sharp peaks associated with specific crystal planes in the structure which allows for phase identification and quantification. The use of a peak indexing software, like the one used in this study (Match!), allows to compare the measured XRD patterns to reference databases and rapidly achieve the identification and rough quantification of the phase in exam. All the samples were measured in the 9-70 ϑ range.

2.7 Scanning electron microscopy SEM

Microscopy is essential to understanding the microstructure of materials, and Scanning electron microscopy (SEM) allows for very high magnification and resolution images. SEM requires that a focused beam of electrons bombard the object to be observed, to be captured by the detectors. This technique utilizes signals of two types, secondary and backscattered electrons. Secondary and backscattered electrons are constantly being produced from the surface of the specimen while under the electron beam however they are a result of two separate types of interaction. Secondary electrons are a result of the inelastic collision and scattering of incident electrons with specimen electrons. They are generally characterized by energies of less than 50 eV. Backscattered electrons are a result of an elastic collision and scattering event between incident electrons and specimen nuclei or electrons. Backscattered electrons can be generated further from the surface of the material and help to resolve chemical contrast. While there are several types of signals that are generated from a specimen under an electron beam the x-ray signal is typically the only other signal that is used for scanning electron microscopy. The x-ray signal is a result of recombination interactions between free electrons and positive electron holes that are generated within the material. The x-ray signal can originate from deeper below the surface and allows for determination of elemental composition through EDS (energy dispersive x-ray spectroscopy) analysis of characteristic x-ray signals. Ceramics, can acquire a strong surface charge due to their inability to conduct the electrons bombarding them. For this reason, it is very helpful to coat

the samples with a thin layer of conductive material, such as gold, which is easily sputtered. Best results were usually acquired with 20kV accelerating voltage and with backscattered electrons, due to the strong chemical contrast between the bentonite and $SrCl_2$. The images were taken on different samples, first the initial powder of bentonite and strontium chloride and then the different scaffolds, from each composition, were observed after failure from the mechanical tests.

2.8 Energy dispersive spectroscopy EDS

Energy-dispersive X-ray spectroscopy (EDX or EDS) is an analytical technique used to probe the composition of a solid materials. EDS makes use of the X-ray spectrum emitted by a solid sample bombarded with a focused beam of electrons to obtain a localized chemical analysis. All elements from atomic number 4 (Be) to 92 (U) can be detected in principle, though not all instruments are equipped for 'light' elements ($Z < 10$). Qualitative analysis involves the identification of the lines in the spectrum and is fairly straightforward owing to the simplicity of X-ray spectra. Quantitative analysis (determination of the concentrations of the elements present) entails measuring line intensities for each element in the sample and for the same elements in calibration Standards of known composition. By scanning the beam in a television-like raster and displaying the intensity of a selected X-ray line, element distribution images or 'maps' can be produced. Also, images produced by electrons collected from the sample reveal surface topography or mean atomic number differences according to the mode selected. The scanning electron microscope (SEM), which is closely related to the electron probe, is designed primarily for producing electron images, but can also be used for element mapping, and even point analysis, if an X-ray spectrometer is added, as the equipment used for the analysis. There is thus a considerable overlap in the functions of these instruments. Chemical composition of the as-fabricated $SrCl_2$ architectures was characterized using Energy-Dispersive X-Ray Spectroscopy (EDS), mounted on the SEM used for the images. Such analysis was only performed on fragments of the 70% composition (both treated and untreated) retrieved after the mechanical tests.

2.9 Ammonia sorption and desorption

The ammonia sorption and desorption performance in terms of ammonia uptake capacity, and the kinetics of ammonia uptake and release are the key factors to evaluate the obtained materials as potential ammonia carriers for SCR systems. The ammonia absorption and desorption performance were characterized by by Prof. F. Akhtar's group at Luleå University of Technology (Sweden) using IsoSORP sorption analyzer (TA instruments, New Castle, DE, USA), which includes a magnetic suspension balance, an electrical heater, a thermostatic oil bath, and a chemistry diaphragm vacuum pump. All samples were degassed at 150 °C under high vacuum for 4 h, following a buoyancy test with helium at 20 °C or 6 hours to determine the mass and volume of each sample. Then, the ammonia absorption capacity was measured with ammonia dosing from vacuum to 3 bar.

CHAPTER 3

Results and discussion

3.1 Sorption evaluations

The porous $SrCl_2$ composites were fabricated using the DIW technique, all the different composites were obtained following identical processing. Notably, the porous $SrCl_2$ structure could be printed with various geometries by changing the code for the DIW machine. Furthermore, the porous $SrCl_2$ bentonite structures composite structures exhibit a wide $SrCl_2$ loading range with porosities which compensates for the volume swing associated with the ammonia absorption–desorption cycles. A series of porous $SrCl_2$ bentonite composites with $SrCl_2$ loading of 60, 70, 80% were obtained. At higher $SrCl_2$-loading, the sample showed lighter color than the lower $SrCl_2$ loaded ones. As the $SrCl_2$ loading increased it can be assumed that the structures during sorpion are more prone to crack at a lower number of ammonia cycles because during ammonia absorption, each $SrCl_2$ molecule theoretically absorbs eight ammonia molecules, resulting in a volume expansion of 400% and a consequent mass increase.

The pore channels in the structure provided the free volume to accommodate the $SrCl_2$ expansion during the ammonia absorption. Furthermore, the scaffold networks have been made to provide some room of expansion, which could contribute to the recovery of the porous structure with a certain strain. The cavities and pore channels permit the accommodation of the volume expansion of $SrCl_2$ particles during ammonia absorption and desorption. Therefore, the $SrCl_2$ particles in the porous $SrCl_2$ composites could "breathe" during ammonia absorption–desorption cycles. Nonetheless, when the $SrCl_2$ loading of the porous $SrCl_2$ composites was too high, the volume expansion and mass gain during ammonia absorption exceeded the volume of the cavities resulting in an irreversible structural disintegration. During the ammonia absorption process, the ammonia molecules first arrived at the surface of the sorbents. After that, they were adsorbed to the surface of the sorbents and diffused into the bulk material, where the surface adsorption has higher energy barriers and lower kinetics compared to the surface diffusion. To enhance the performance a higher permeability is necessary to achieve a rapid ammonia transport with higher mass transfer. Aside from the surface adsorption sites, the diffusion length of the sorbents can impact significantly the net absorption–desorption dynamics, since ammonia absorption and desorption in AEMHs are highly diffusion controlled, and lastly, many mechanisms, including but not limited to diffusion controlled by surface resistance, could influence the uptake kinetics.

A possible schematic mechanism of the adsorption can be as follows:

- transport of the NH_3 molecules from the atmosphere to the boundary layer;
- diffusion of molecules through the boundary layer;
- adsorption of the molecules on the surface;
- formation of the complexes;
- the adsorbed NH_3 enters the structure;
- possible growth of the complex structures;
- diffusion of the NH_3 from the substrate to the core material.

The adsorption evaluation were performed only on the 70% composition (with and without heat treatment), the adsorption curves data of the 70% composition without heat treatment are shown in Fig 3.3, showing that after 9 cycles of adsorption and desorption the structures did not lose any of their sorption characteristic, achieving for each cycle an uptake of 600 mg/g or 37.8 mmol/g. As said before the adsorbtion is followed by an increase in volume of the network, the reticular structure of the scaffold was chosen to accommodate this increase but as Fig. 3.2 shows, the first crack propagates through the piece at the mark of the third cycle and complete fracture occurs at 6th mark, but still not hindering the adsorption properties. Fig. 3.4 reports the adsorption performance of the 70% composition heat treated at 800°C: as shown in the graph the uptake reaches only a maximum of 140 mg/g, because of severe modifications in the microstructure of the sample.

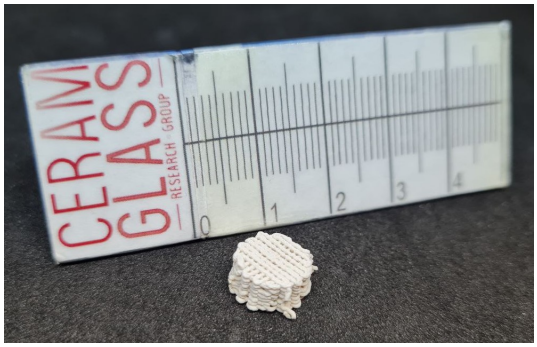

Figure 3.1: Ammonia sorbent

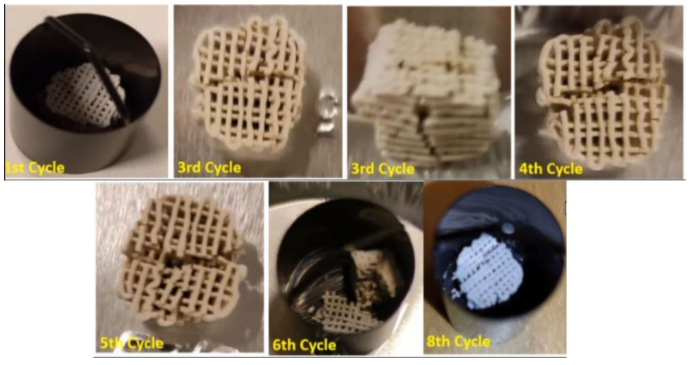

Figure 3.2: Ammonia sorbent after marked cycle

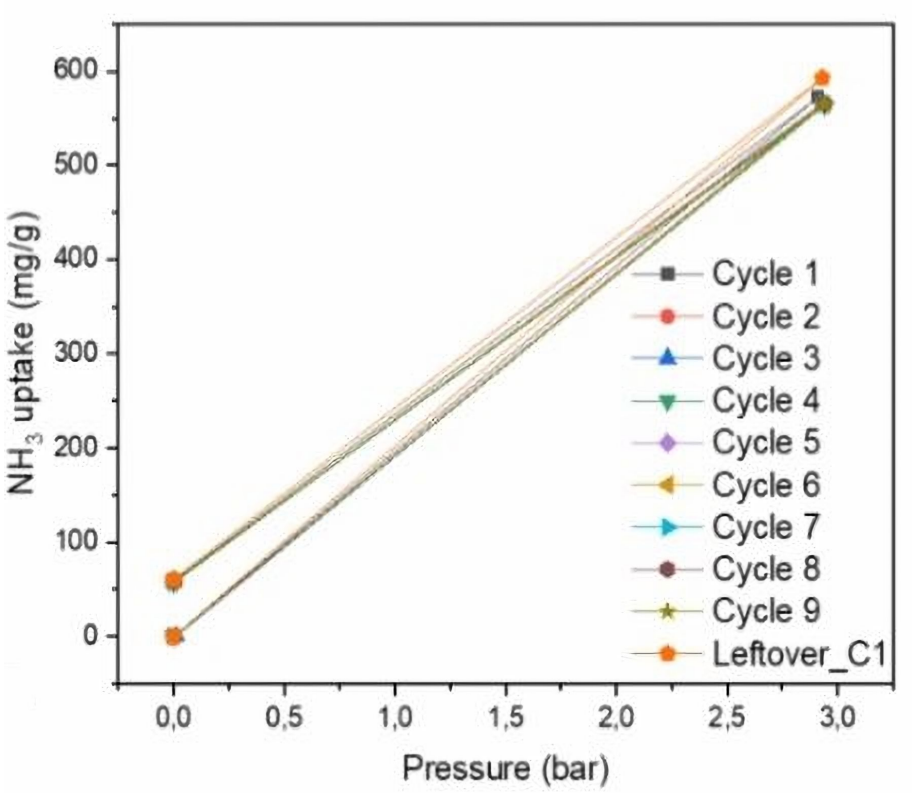

Figure 3.3: Ammonia uptake of the 70% composition with no heat treatment

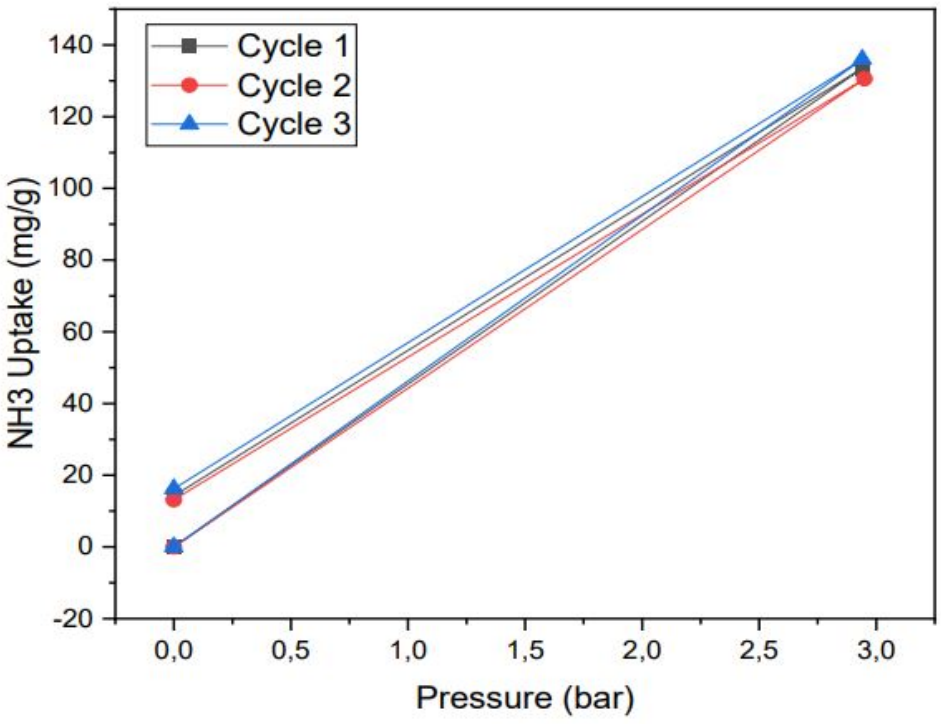

Figure 3.4: Ammonia uptake of the 70% composition treated at 800°

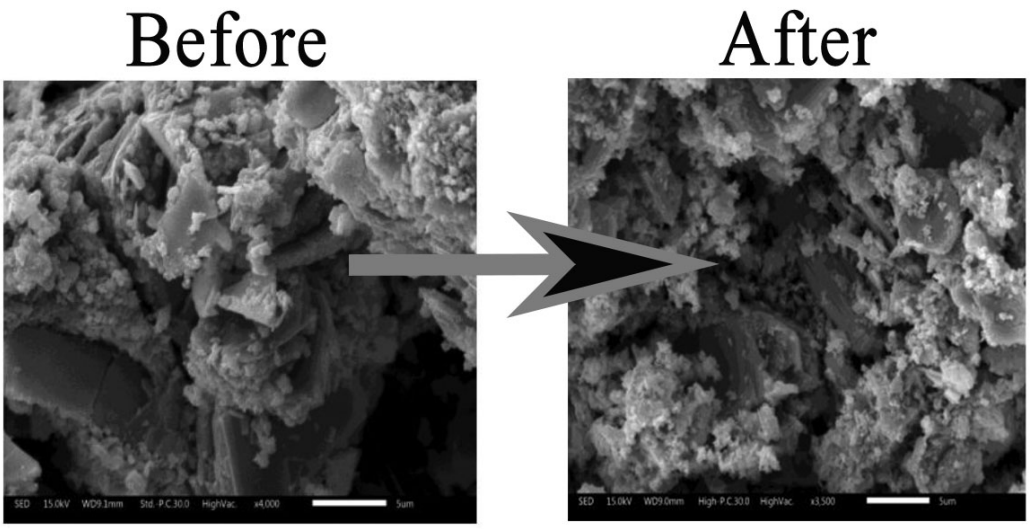

Figure 3.5: SEM images of the samples before and after adsorption, treated at 800°

Fig 3.7, shows that the samples heat treated did not show a drastic expansion after the adsorption experimentation, as the theory had suggested, but we can see the small clusters after the adsorption get more powder like, this because the heat treated structures could be made of a combination and strontium chloride, a less efficient adsorber.

In general stress and strain are generated in porous solids when matter adsorbs on the pore surfaces. The solid may be in contact with gas, where the vapor pressure of the adsorbate controls the adsorption process. Alternatively, the solid may be in contact with a solution containing the adsorbing species in the form of dissolved molecules or ions, in which case a chemical or electric potential controls the adsorption. In simple scenarios the fluid (vapor or solution) extends uniformly from the outside of the porous solid into the pore space. The solid is then loaded by the combination of the hydrostatic pressure of the fluid and by capillary forces that act along the pore walls. Here, menisci form between the outer fluid and the liquid in pore space. This leads to a mechanical loading scenario in which part of the solid surface is loaded by the pressure in the liquid, while simultaneously capillary traction forces act at the liquid-solid-vapor triple lines and the liquid-solid interfaces experience surface stress until failure occurs.

As we understand mechanical integrity is very important aspect of the sorbents when developing it for a possible industrial application, so mechanical analyses was performed to evaluate the structural performance of the sorbents. By optimizing the ink, this approach might provide ways to design stable structured sorbents to accommodate the volume expansion and shrinkage associated with absorption and desorption, respectively, as well as introduce the synergic advantages from the networks.

3.2 Mechanical performance

As shown in chap. 2 the compression mechanical performance was evaluated by means of Weibull model. The Weibull modulus determined from the strength data for a large number of identical samples (typically 20-30 or more) is commonly used as a measure of the mechanical reliability or the probability of failure of brittle materials. The mechanical response of brittle materials is sensitive to microstructural flaws such as pores and micro-cracks: therefore, Weibull modulus is used to evaluate the probability of failure of brittle materials under a given stress. In this work, the Weibull modulus of scaffolds produced with $SrCl_2$ was assessed for the first time, hence a direct comparison with analogous data from the literature is not possible; nonetheless, a few results concerning scaffolds produced by different techniques can be considered.

Survival probability curves of the different composition under the same condition of compression test. For each composition a different number of specimens were tested giving more validity to the ones with more population. The tables with all the dimensions and the fracture stresses of the samples are reported in Appendix 1 (Tab. A.1-A.2-A.3-A.4) pag. 63. In Tab. 3.1 all the characteristic parameters of the scaffolds tested are shown.

Population	Composition	Weibull Modulus, m	Scale Factor, σ_0 (MPa)
8	**70-30HT**	12,1	1,3
7	**70-30 NOHT**	2,9	2,1
15	**60-40**	2,58	4,3
16	**80-20**	1,94	0,26

Table 3.1

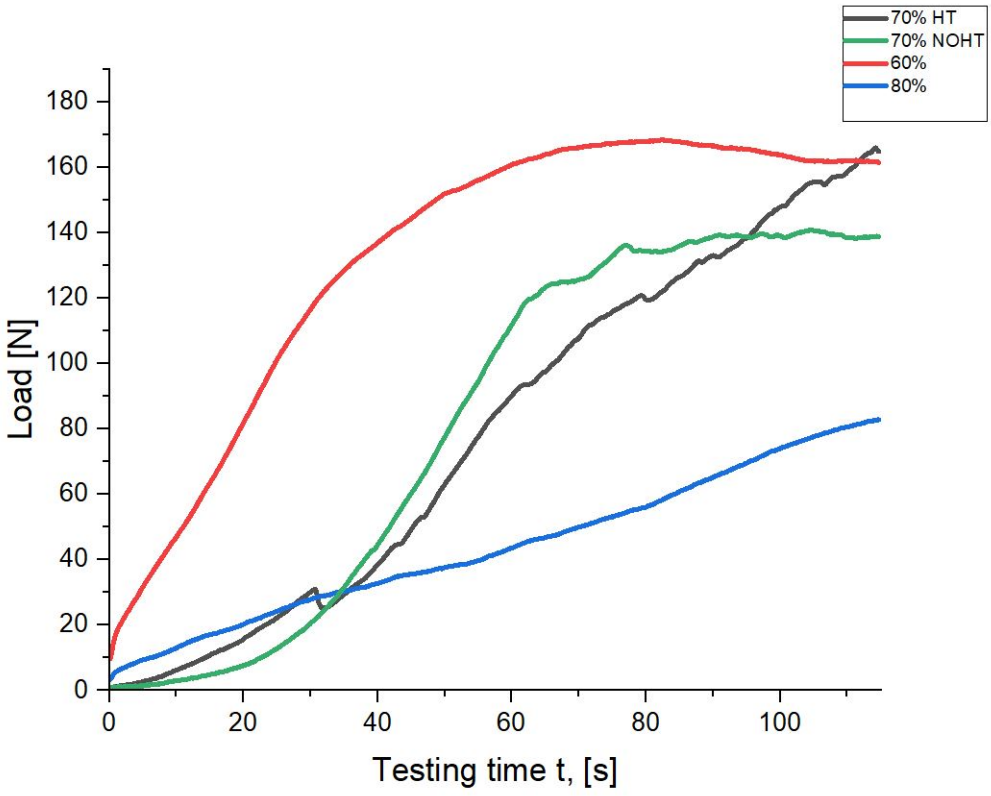

Figure 3.6: Uniaxial stress curves of typical samples for each composition

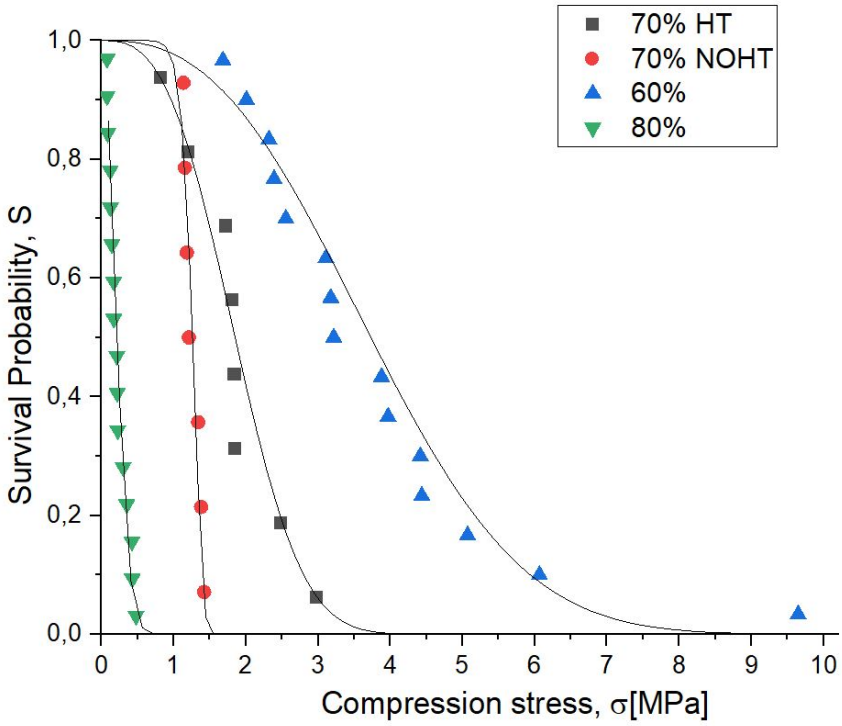

Figure 3.7: Uniaxial stress curves of typical samples

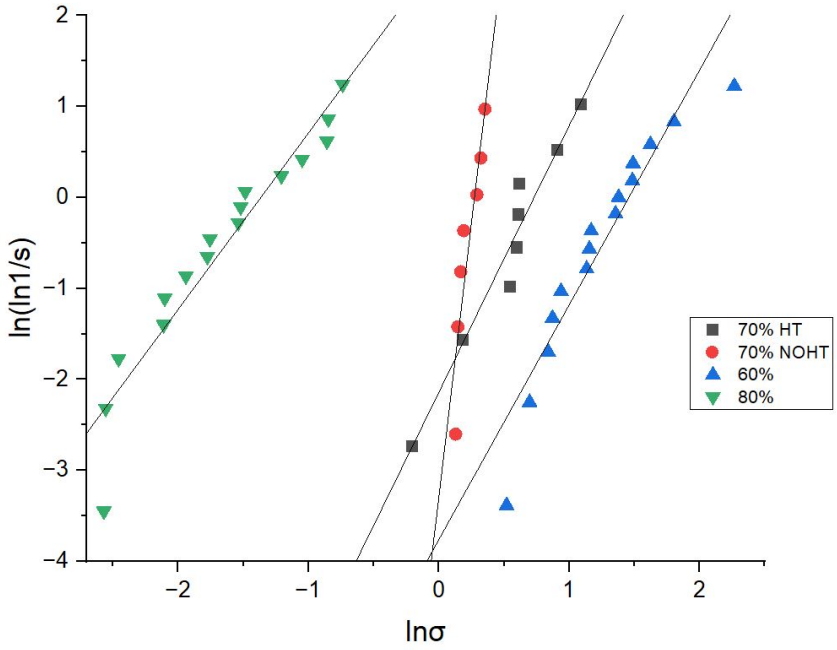

Figure 3.8: Linear regression data to estimate Weibull modulus and scale factor

There were considerable variations observed for the mechanical response of individual scaffolds taken from each batch of scaffolds fabricated. This can be clearly seen in the S curves obtained from testing several $SrCl_2$ structures shown in Fig. 3.8. However, all of the compression tests show the same features. There is always a region at the beginning of each test showing a small increase in stress with increasing compressive strain. This is followed by a region of linear elastic deformation before discontinuities occur above a stress that is different for each scaffold, these are believed to indicate internal sub-critical fracture of individual struts, before peak load and final crushing occurs. It is notable that like the behaviour of many brittle structures there is a distinctive plateau region of constant crushing strength after peak load, and after there is a regime of increasing stress or densification at large strains Fig 3.6. The peak stress or crushing strength data are reported in the Tab. A.5-A.8 ranked by ascending fracture stress, along with the Weibull modulus, for the scaffolds tested. Assuming that the mechanical properties of the scaffolds are described by the model of Gibson and Ashby for the properties of cellular solids, the strength of a strut in the scaffold is the same as the strength of the bulk material and is related to the strength of the cellular solid (scaffold) by its relative density with:

$$\frac{\sigma_{cell}}{\sigma_{bulk}} = 0,65(\rho_R)^{1.5}$$

where ρ is the relative density (1 - porosity) of the cellular solid. This computed structural strength is also shown. From Table, it is clear that the Weibull modulus values for all scaffolds are low. Conventionally, one would expect Weibull modulus values of solid ceramic specimens to range from 5 to 20. However, other researchers have also found low values of Weibull modulus for ceramic and glass biomaterials. Others reported Weibull modulus values in the range 2–4 for bioactive glass and Weibull modulus of 4 for glass ceramic scaffolds. For other brittle foams, the literature values for the Weibull modulus are also low, e.g. in alumina foams the Weibull modulus is reported to be in the range of 1–3, and for reticulated vitreous carbon foams in the range of 4.4–6.2. [12][13]

Survival analysis is a branch of statistics designed for analyzing the expected duration until an event of interest occurs. In general, our “event of interest” is the failure of a structure. We denote the compression stress at which this structure fails by σ. The survival function S(σ), merits special attention as it is one of the most useful and intuitive statistics associated with survival analysis. The survival function is simply the probability that the scaffold will fail as a stress σ is applied, or equivalently that it will still be in service at that stress. As the load increases, it becomes more and more likely that the structure will fail in the next period given that it has lived until the current period; therefore the hazard function in the example above steadily increases. And it becomes less likely that the structure will still be "alive" after each successive period, which is why the survival function for the same hypothetical structure decreases as the stress increase. From these graphs it is possible to have a better understanding on how the Weibull function works and be able to asses in which range of stresses the monoliths with different composition will fail.

Starting from the 70% composition without thermal treatment, it can be seen from Fig. 3.9 how all the specimens of this composition failed more all less on the same compression stress around 1-1.5 MPa. This could be related to a more homogeneous structure of the monoliths and so on the they show more or less the same performances. This composition is characterized by a Weibull modulus (m) of 2.9, in general the higher the Weibull modulus is, the more consistent the material (which means that uniform "defects" are evenly distributed throughout the entire volume) and also the narrower the probability curve of the strength distribution. The scale factor was calculated to be 2.1 MPa

For the 70% composition heat treated, we can see from Fig. 3.9 how all the specimens failed on a wider window of stresses around 1 to 3 MPa. The heat treatment increased the

performance of the structures due to densification of the lattice, improving the mechanical performance but severely reducing ammonia uptake, as shown in the previous section, so for the compositions 80% and 60% no thermal treatment was applied. The Weibull modulus (m) is 12.1 and the of 1.3 MPa, showing the highest modulus means that dispersion is distributed in a broader range.

For the 60% composition the Weibull modulus (m) is 2.58 and the scale factor σ of 4.3 MPa. As the tested population increased it is possible to appreciate a broader range of compression stresses, that reaches even the 10 MPa, awhile minimum fracture stresses increase to about 2 MPa. From this we can understand that loading the structure with more bentonite increases the mechanical performance considerably.

For the 80% composition, Weibull modulus (m) is 1.94 and the scale factor σ is 0.26 MPa, the lowest between all compositions. From all the batches this is the one with the lowest performance as shown in the graph where the compression stresses varies in narrow range between 0.1 to 0.5. It must be noted that for this the evaluation of the mechanical data was difficult as the structures failed at very low stress and a clear indication of fracture was not always evident in the stress curves, as shown Fig 3.8.

Lastly it can be said that compressive strength of the $SrCl_2$-bentonite increased with addition of the bentonite by lowering the content of $SrCl_2$. This behavior can be explained possibly by the bentonite producing two effects: its inherent higher strength compared to the pure $SrCl_2$ and the beneficial effect of the improved rheology of the slurry that gave more homogeneity to the cell, so the use of icreased bentonite results in scaffolds with higher strength over the $SrCl_2$ alone. With further increase in the $SrCl_2$ content, the structures exhibit a very brittle cell structure, mainly for the poor mechanical characteristics of the salts, leading to a rapid decrease in strength and modulus. [14]

3.3 EDS compositions

The EDS evaluation were obtained from the same device for the SEM-EDS analysis. The only compositions studied was the 70% at the sintered and not sintered conditions. Each "snapshot" taken with the SEM had multiple EDS data, easing the evaluations of the area composition and the detection of the predominant component in each phase. The EDS was performed 5 times in different sample areas as follows:

- Strontium Chloride powder;
- 3d printed 70% no heat treatment sorbent confrontation between different filaments;
- 3d printed 70% no heat treatment sorbent one filament;
- 3d printed 70% heat treated sorbent one filament;
- 3d printed 70% heat treated sorbent focus on phases of printed filament.

In the next pages all the reports are attached and all the qualitative evaluation are based on the intensity of the peaks related to the different elements.

The first report is about the pure $SrCl_2$ powder as freshly out of the bottle, two different spots were studied in which a visible color shade difference could be addressed:

- spot 1 is on a clear powder crystal;
- spot 2 is on a darker powder crystal;

The report suggests that the composition of the two is different, the first spot could be associated with a $SrCl_2$ crystal as the main peaks are Sr and Cl, for the second spot the evaluation is more complex as the Sr peak is overlapped with the Si, however as we know the origin of the powder the misidentification can be ascribed to software error. It must be noted, however, that the peak of oxygen is very pronounced probably indicating a higher content of complexed water molecules on the crystal. The analyses suggest that the powder batch used for the experiment is a mix of different degrees of hydrated Strontium chloride.

The second report is about the section of the 3D printed untreated 70% sorbent, it underlines how the composition pattern is in each section of the filaments. From a theoretical point of view each monolith was printed with the same ink and so the composition would be consistent in each part of the sample and it would reflect both the presence of bentonite and strontium chloride with the characteristic elements Sr, Cl, O, Na, Al, Si and H. Composition was analysed in four areas, progressively located more closely to the external surface of the monolith. For all the areas the composition matches the presence of the elements of both bentonite and strontium chloride, but as before there are problems addressing which peak is related to Sr and Si. The most interesting thing about this evaluation is the fact that the strontium crystals become more visible on the more external filaments, this is evident from Fig 3.10, the outer filaments are characterized by a lighter color possibly associated with the presence of the salt. The reason for this difference in morphology is difficult to address, as said before all the inks were prepared by mixing and this implies the fact that the compositions would be homogeneous, from a material science perspective thinking about the possibility of diffusion mechanism happening at this scale in a open structure is difficult, the only thing that can be said is related to the drying process: the outer layers will be the first to fully dry while the more internal ones will be the last, this may be associated with the possibility a preferential recrystallization of the salt.

The third report analyses the section of a filament of the untreated 70% sorbent. This report shows very clearly the real composition of the structure as the main peak is the one of Sr followed by Cl and Si in a percentage that looks pretty real.

The fourth and fifth report concerns the composition of the sintered sorbet 70%. From the SEM image of the fourth one it is possible to appreciate some lamellar phase, inside the matrix and more elongated crystals that were not present before the heat treatment. Three spots and an area were analysed:

- area 1 and spot 3 on the homogeneous matrix;
- spot 2 is on a elongated crystal;
- spot 1 on the lamellar phase;

Looking at the different patterns it can be said intuitively that all of them contain both bentonite and strontium chloride elements and the new evolution of the microstructure is due to the transformation of some unidentified strontium aluminosilicate.

The fifth and last report is a more focused analysis on the needle-like complex crystals that grow after sintering to understand if one of the two components is more predominant. Four spots were analyzed: spot 1 is on the tip of a crystal and shows a 100% presence of strontium chloride, while the others still show the presence of elements related to bentonite. This may suggest that the needles are a recrystallization of strontium chloride that appeared after heat treatment as it is known in literature [15] that $SrCl_2$ can assume such shape, or they might be a mix of bentonite and strontium chloride.

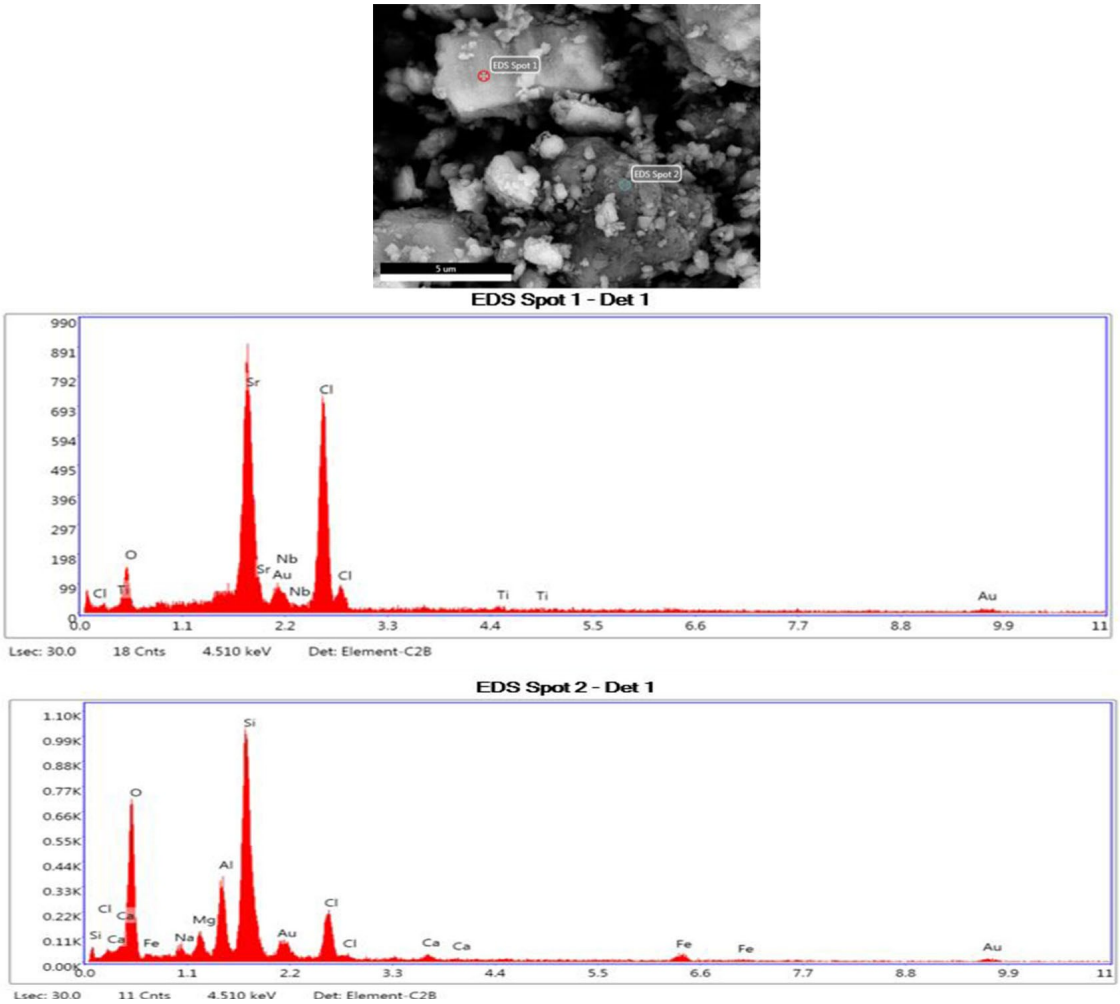

Figure 3.9: Strontium chloride powder

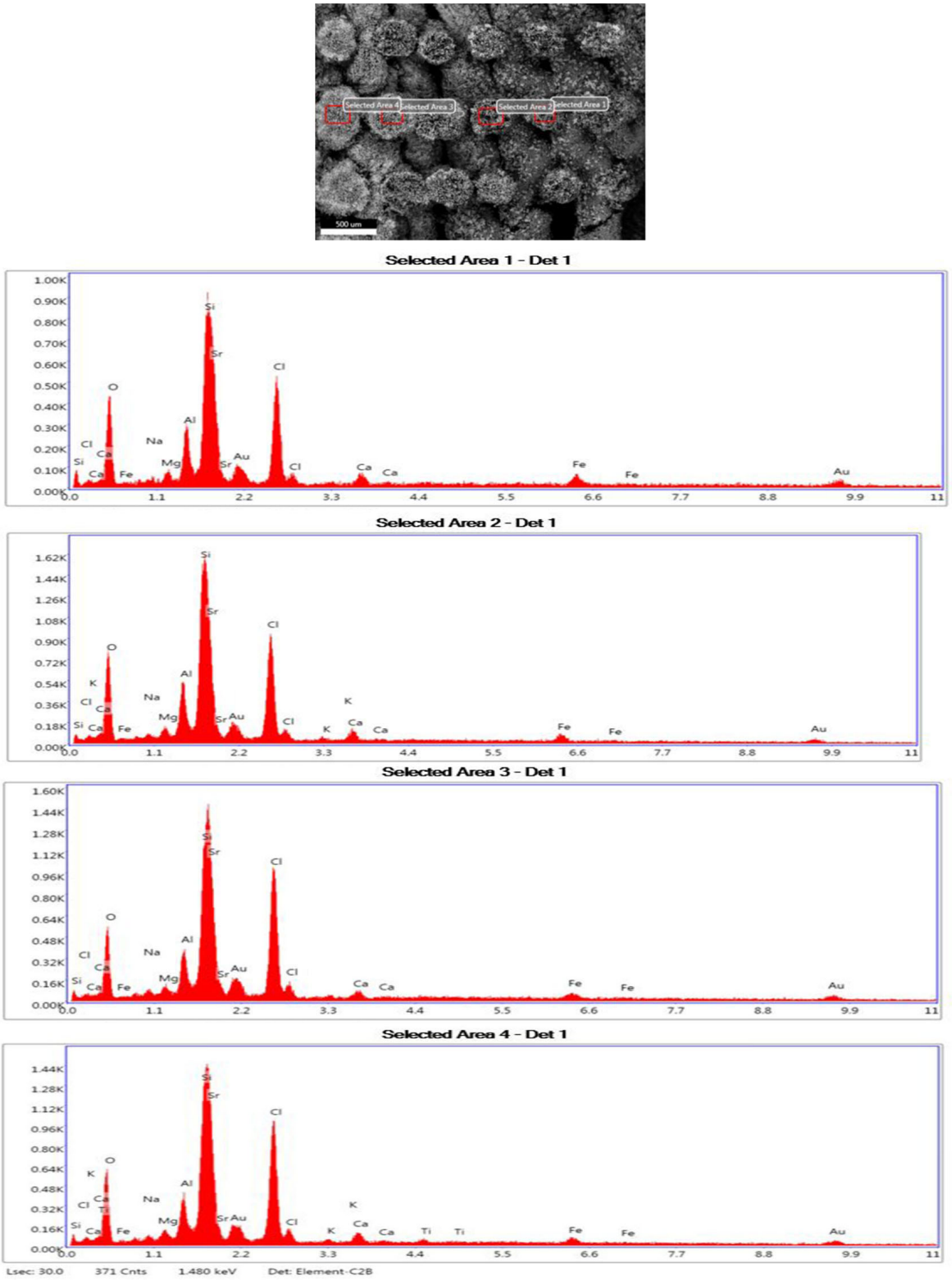

Figure 3.10: 3d printed 70% no heat treatment sorbent confrontation between different filaments

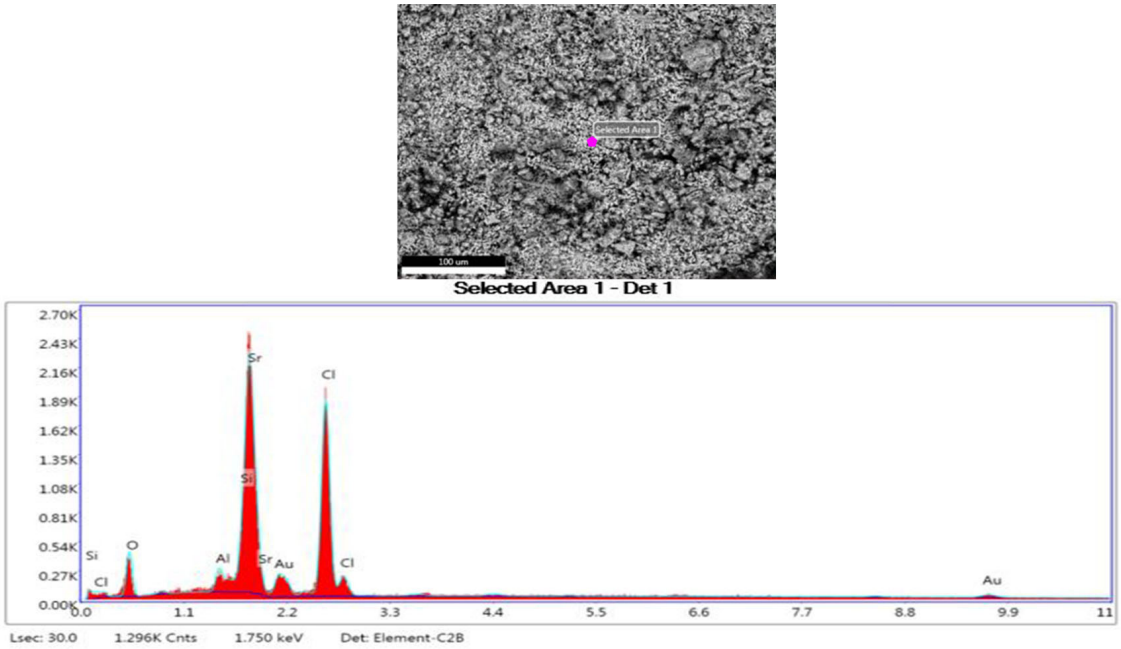

Figure 3.11: 3d printed 70% no heat treatment sorbent section of a filament

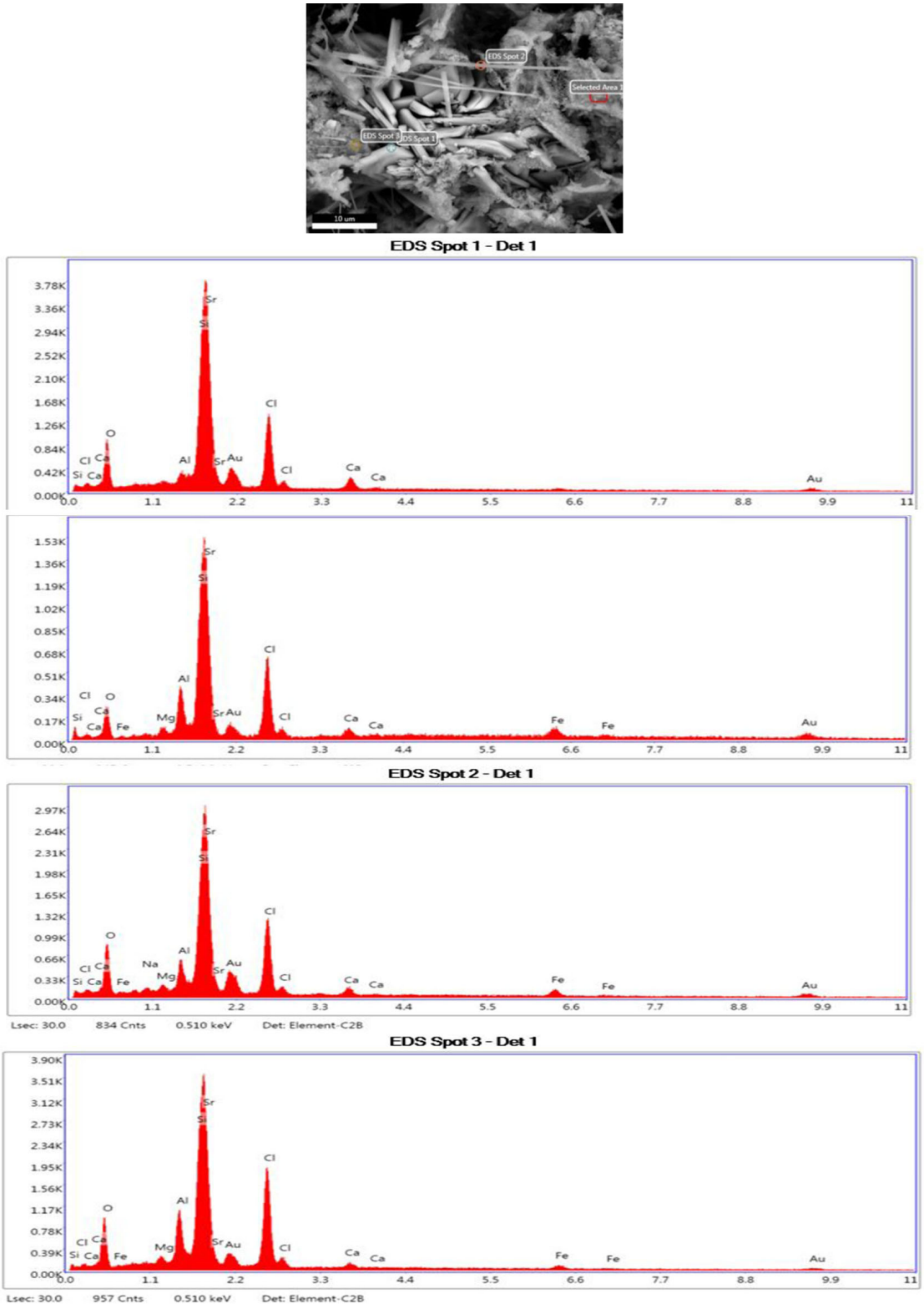

Figure 3.12: 3d printed 70% heat treated sorbent surface filament

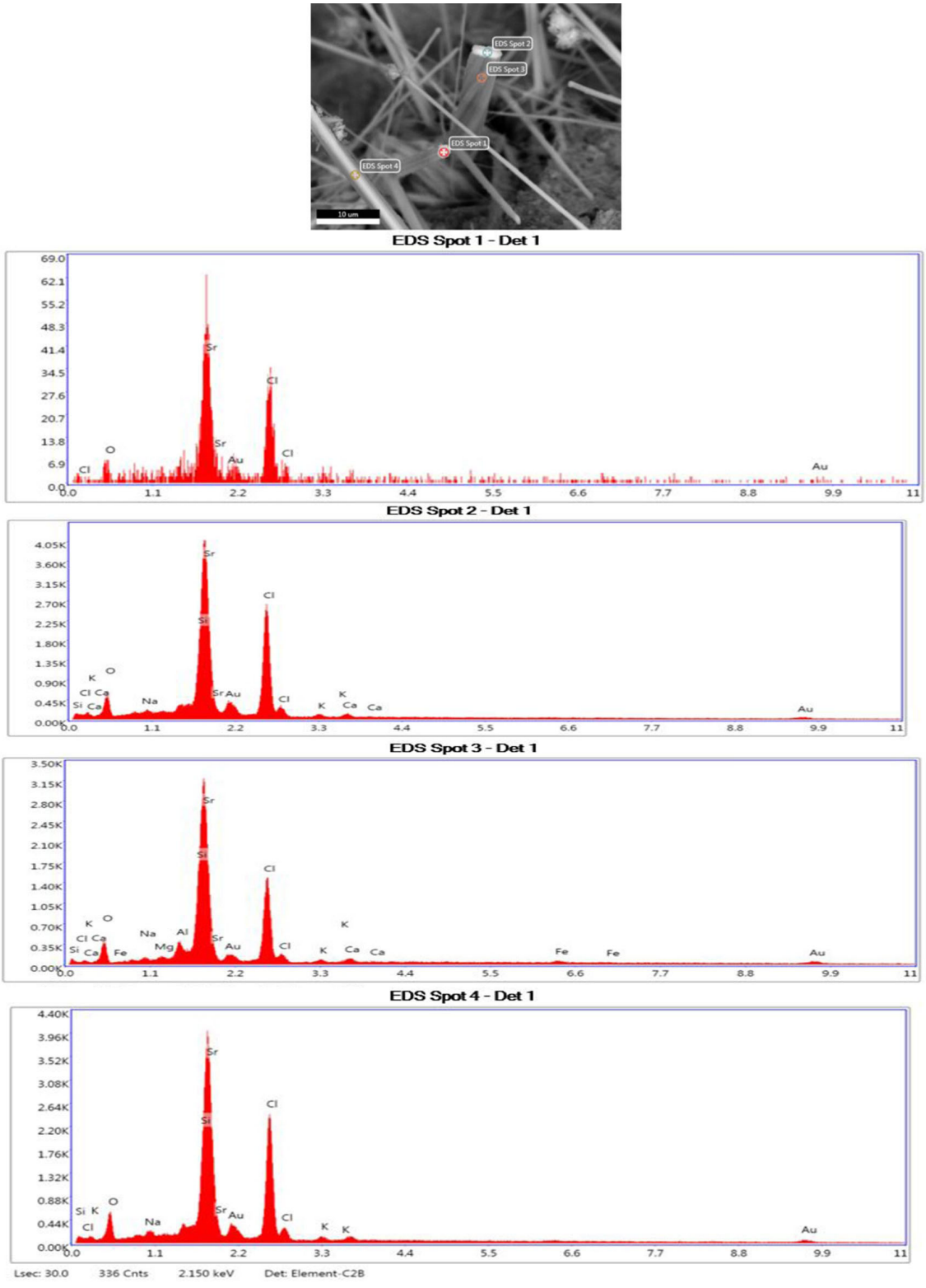

Figure 3.13: 3d printed 70% heat treated sorbent focus on phases of printed filament

3.4 XRD patterns

The results of the characterization of $SrCl_2$ bentonite by X Ray Diffraction are shown in the next page. The patterns look very complex as the matrix is made of $SrCl_2$ and bentonite that is composed of 4 types of mineral.

The characterization of the samples by XRD aimed to verify the existence of associated minerals, clay minerals and strontium chloride. Fig. 3.16 presents the X-ray diffraction results of the samples studied in the present work. The XRD patterns show the presence of montmorillonite (6.7, 23.21, 42.08 and 73.82°), kaolinite (14.42, 29.05, 40.90, 44.07, 59.94 and 65.06°) and strontium chloride (as reported in Fig. 3.18-3.19) as major phases.

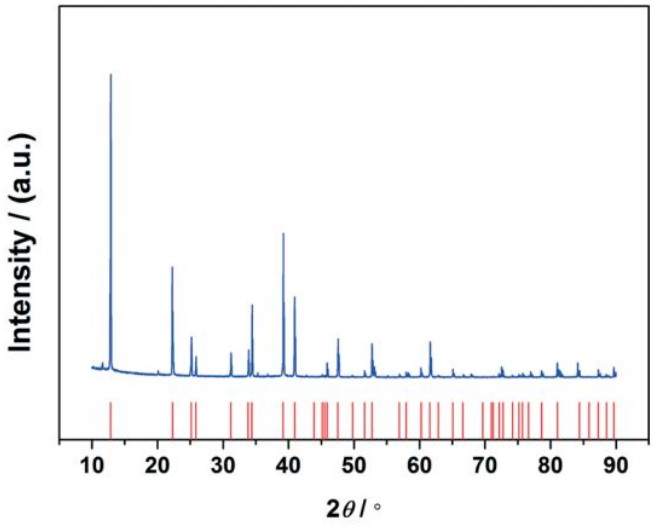

Figure 3.14: XRD pattern of pure $SrCl_2$

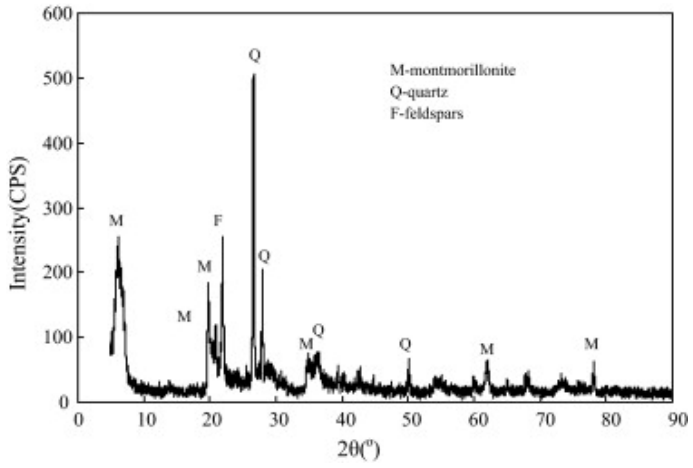

Figure 3.15: XRD pattern of pure bentonite

XRD patterns indicate that the data obtained from samples with different composition are consistent and show more or less the same peak pattern; only for the treated one a drastic structural change is observed, this strengthens the EDS analysis evaluation on the effects of the thermal treatment on the 70% composition. The last two patterns show how much the printed samples deviate from the data of the powder, the peaks overlap, but for the 70% composition the raw powders display higher intensity than the printed samples, while in

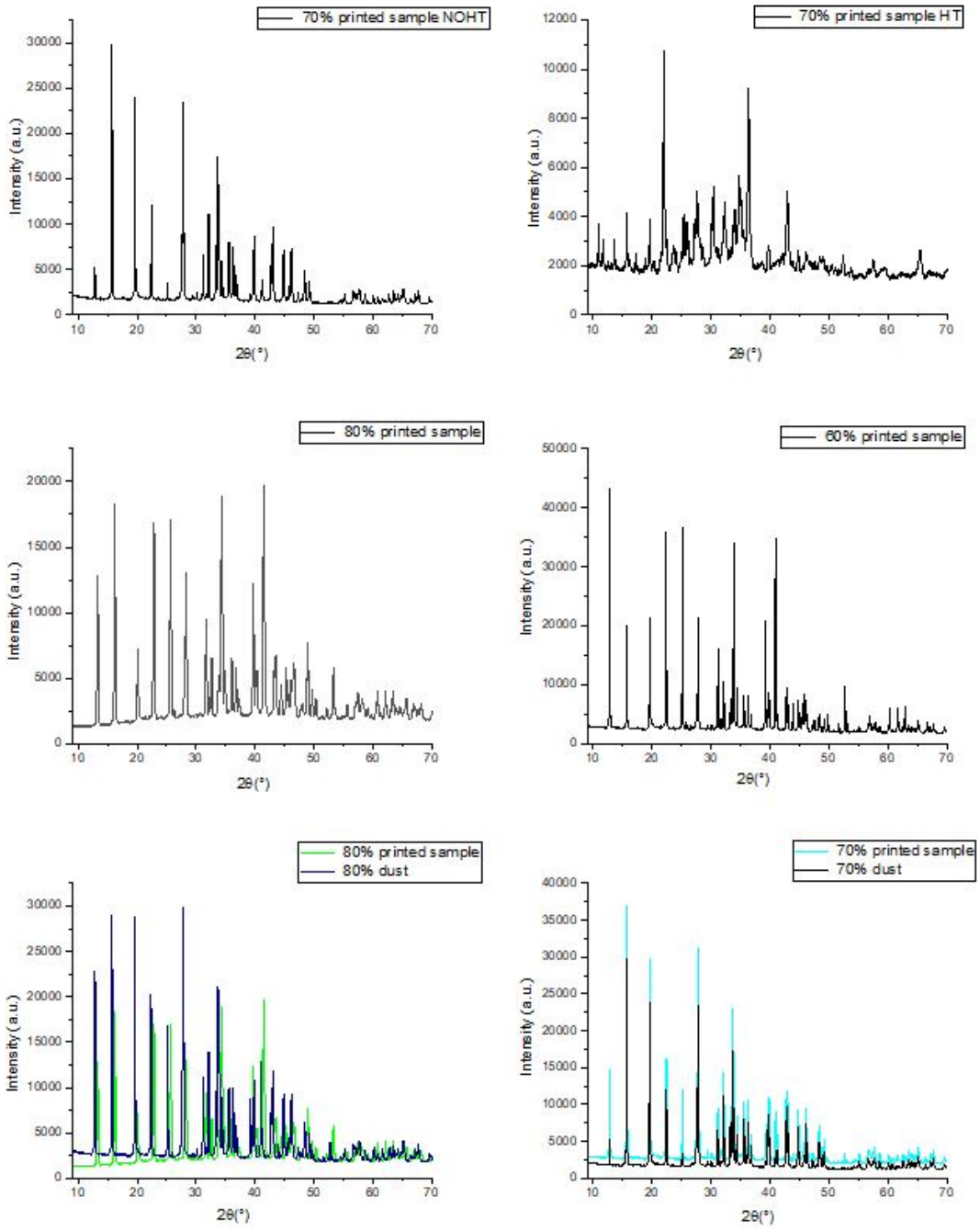

Figure 3.16: XRD patterns of all the sample analysed

the 80% the opposite occurs, this behaviour is probably related to the homogeneity of the raw dusts used for the XRD. The two top graphs in Fig. 3.16, relating to the untreated and treated 70% sample, indicate massive microstructural modifications occured with the heat treatment; moreover, the pattern for the treated sample has considerably lower intensities and more prominent background, indicating that crystallinity may be lower.

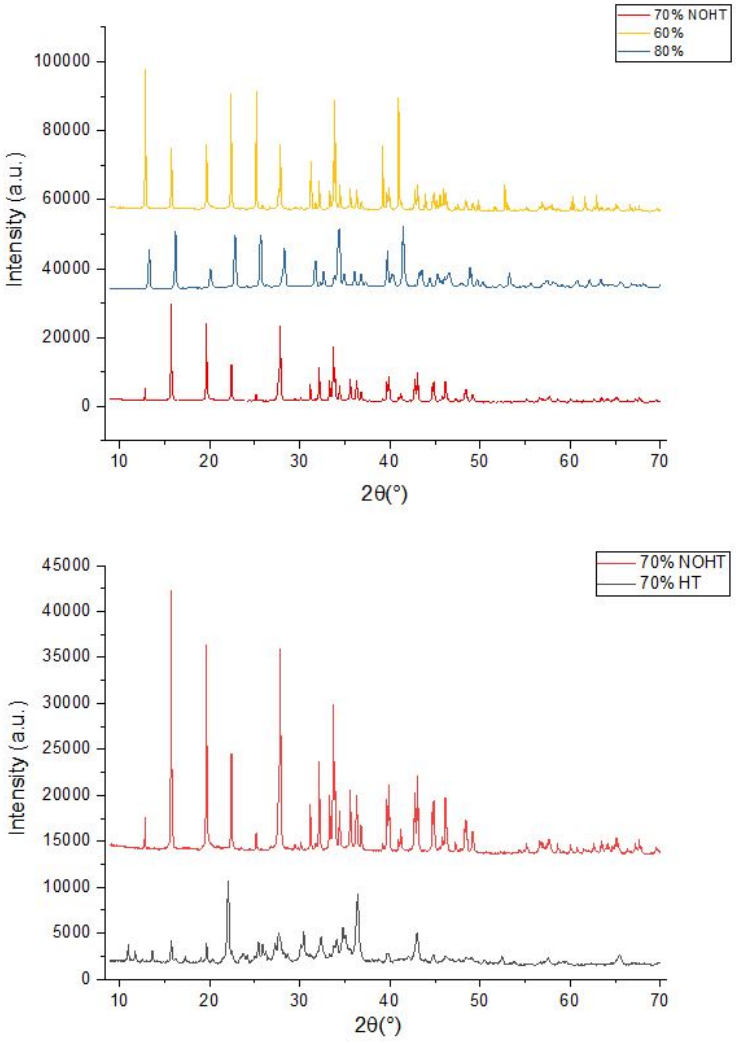

Figure 3.17: XRD patterns of all the sample analysed

3.5 BET analysis

All the isotherms of all compositions are shown in Fig. 3.18-3.19-3.20. From looking at the one that regards the 70% composition we can easily understand that the underlying treated sample shows no adsorption underlying the fact that the thermally treatment hinders the porous characteristic of the material. All three of the isotherms for the untreated composites have the same shape, which can be identified as belonging to a type IV isotherm with a H3 hysteresis loop according to the IUPAC definition. This indicates that the samples are mesoporous, and the presence of a limit uptake at high p/p_0 suggests that macroporosity is limited. Tab 3.2 collects all the data obtained from the BET analysis, as we can see that the highest SSA (Specific Surface Area) is shown by the 60-40 and 80-20 composition, while the 70% has an intermediate value and the treated 70% shows the lowest value. Looking instead at the pore volume, the highest value are found in the 60-40% and 80-20% structures and as before the 70-30% untreated has an intermediate value while the treated 70-30% shows a drastic decrease of the volume with respect to the untreated one. From the data reported about the 70% composition it is clear that the thermal treatment nullifies the porous properties of the structure by severely reducing both SSA and pore volume. The 60% composition shows the widest loop, but as the fraction of $SrCl_2$ increases the loop starts reducing and the isotherm shifting to a more type-III character, compatible with the pure salt being essentially non-porous.

The type H3 hysteresis loops depicted are typically given by the adsorption of nonpolar gases by montmorillonite clays and the aggregates of other plate like particles. It is evident that these H3 loops have characteristic desorption shoulders and lower closure points, which in the case of N2 adsorption at 77 K are located in the region of $0.42P_0$. However, the H3 loop does not have a plateau at high P/P_0 values and therefore this form of isotherm should not be referred to as type IV. Since there is no well-defined mesopore volume, caution should be exercised in the interpretation of the uptake at high P/P_0. Although only the initial monolayer–multilayer section of the isotherm is reversible, the whole adsorption branch of the H3 loop appears to exhibit the same shape as a type II isotherm. This pseudo-type II character is associated with the metastability of the adsorbed multilayer (and delayed capillary condensation) and is due to the low degree of pore curvature and non-rigidity of the aggregate structure. The shape of the H3 loop is also linked with the non-rigid nature of the adsorbent and the location of the characteristic shoulder is consistent with the destabilization of condensate at the limiting P/P_0 value. [16] As we know the salt does not increase the surface area but a high SSA is showed by the 80% composition, For the pore volume all the compositions are more or less the same and a relation with the composition can not be found.

	BET SSA (m^2g^{-1})	Pore Volume (cm^3g^{-1})
70-30 HT	<1	0.007
70-30 NOHT	10.4	0.055
60-40	17.209	0.063
80-20	16.716	0.077

Table 3.2

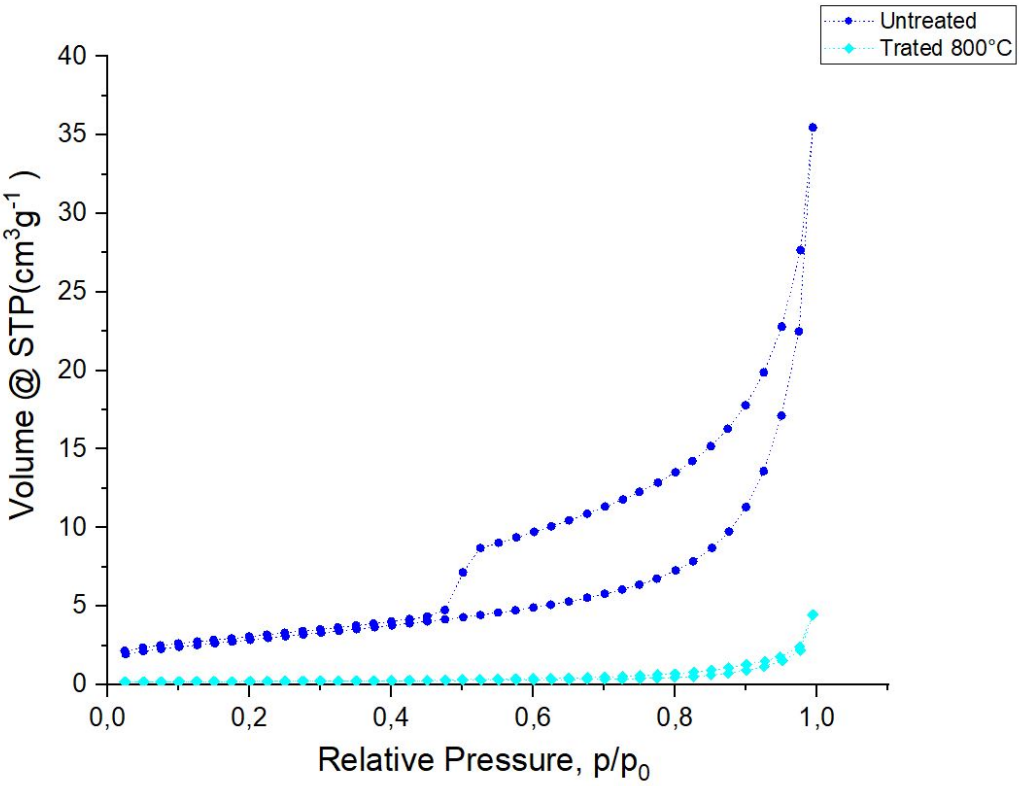

Figure 3.18: BET curve for 70% NOHT-HT

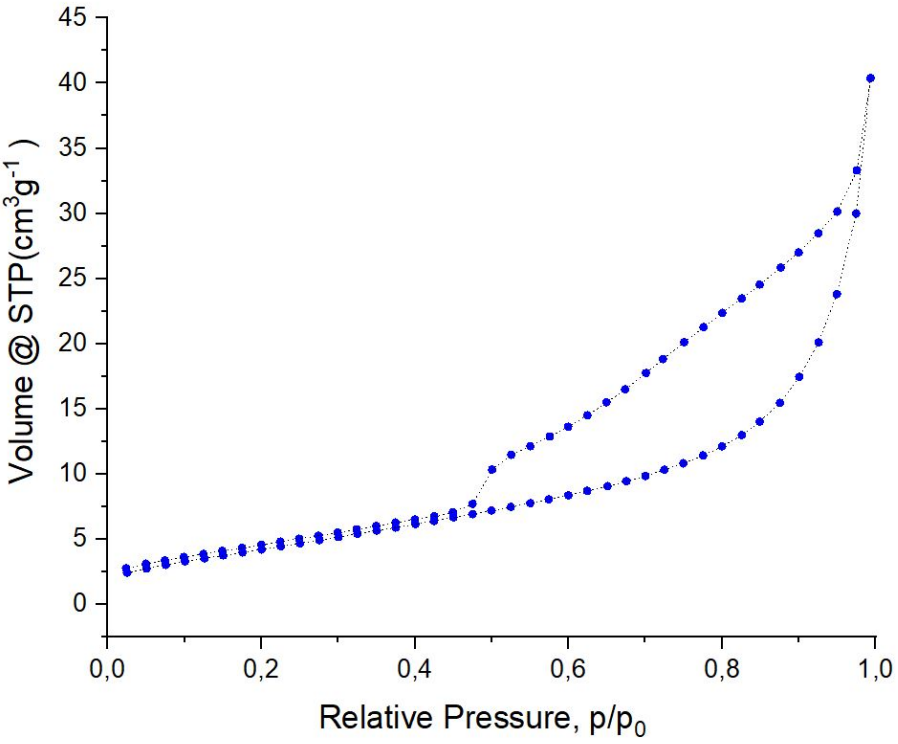

Figure 3.19: BET curve for 60%

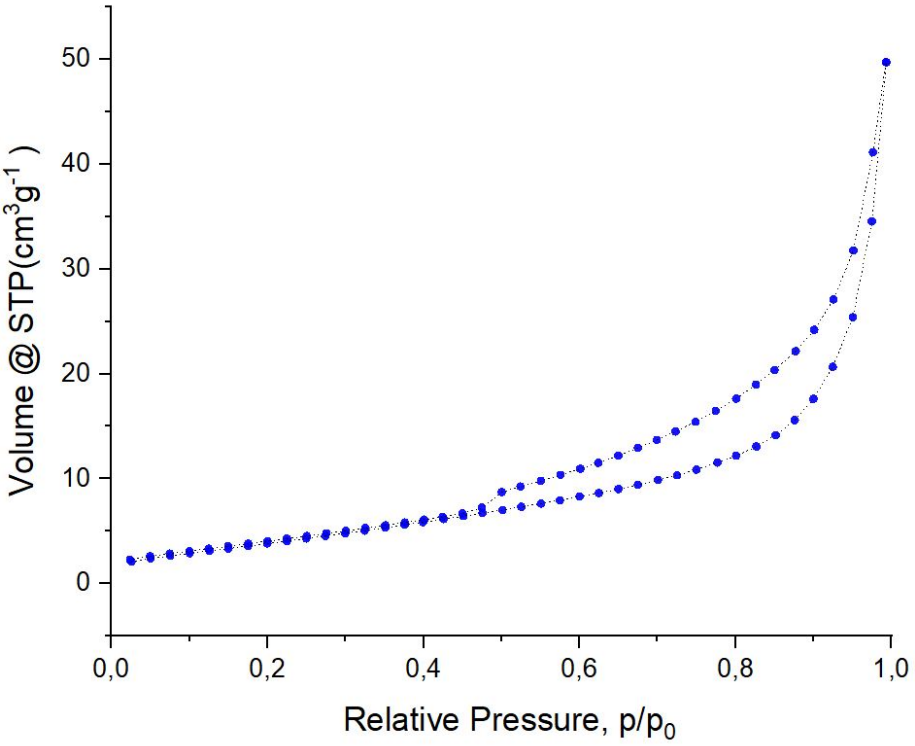

Figure 3.20: BET curve for 80%

3.6 SEM images

3.6.1 Raw materials

The as received crystals Fig 3.21 $SrCl_2$ before milling have different size, spanning a few order of magnitudes. Particle size is a very important factor in colloidal science because it determines the ratio of surface area to mass of powder. Through this, either the electrical forces at the surface or gravitational forces due to mass will dominate, determining the ability of particles to be suspended indefinitely. Grain size is also a key element in sintering, as nanoparticles can have significantly reduced energy demands to produce fully dense parts as compared to conventional micron-scale particles or larger. For the purpose of this study the powder had to be smaller than 1/10 of the nozzle diameter in order to avoid clogging during printing and other factors were not taken into account.

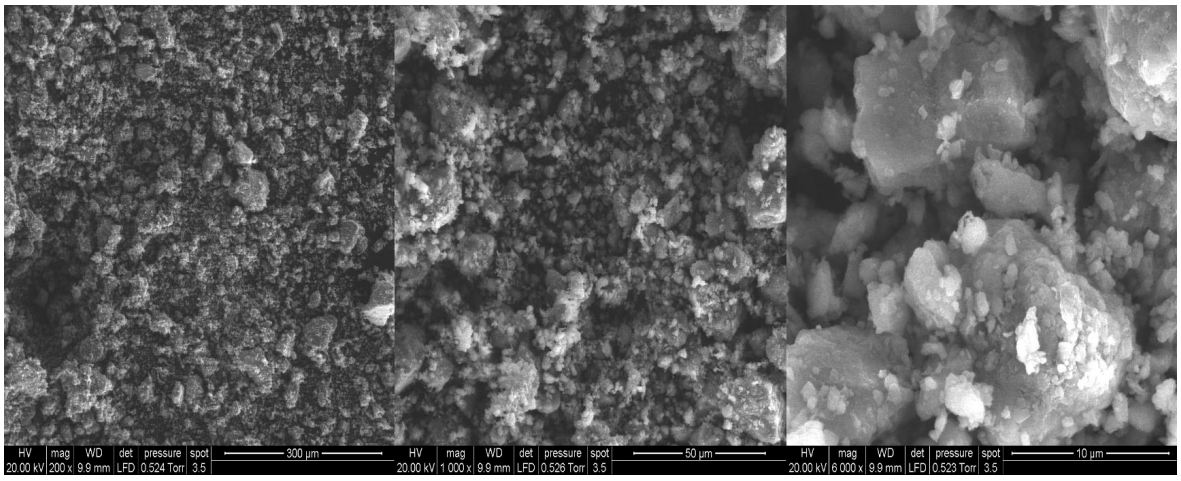

Figure 3.21: SEM picture of $SrCl_2$ salt, left to right, 200x - 1000x - 6000x

In addition to powder composition, the shape and size of powders is very important in defining final properties of built parts. In order to gain insight into powder morphology, the as-received powder was scanned by Field Emission Scanning Electron Microscope , and result is presented in Fig. 3.22. As the figure shows, powders have both spherical and irregular shapes with a wide variety of dimensions. In fact, general dimension of powders starts from some microns and goes up to 50 microns.

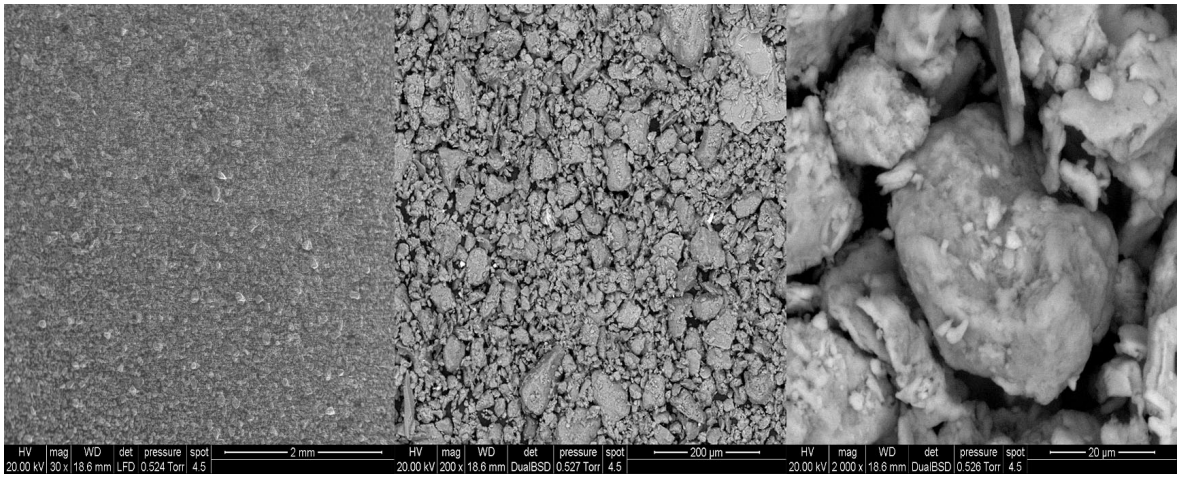

Figure 3.22: SEM picture of the Bentonite powder, left to right, 30x - 200x - 2000x

Surface morphological analysis of the strontium chloride based composites were done by scanning electron microscopy (SEM). Observation was carried out by both secondary electron and back scattered electron imaging techniques, operated at an accelerating voltage of 15-20 kV.

3.6.2 70% composition

The first set of image presented are ones from the fracture surfaces of the filaments of the 70% composition all of which have been taken in BSE mode, as it enhances the contrast between the matrix and the $SrCl_2$ clusters that are more white colored. The images show that the clusters are present in different dimension, ranging 10 to 30 µm. In the 250x image small platelet-shaped structures can be appreciated, from the contrast with the background they could be associated with strontium chloride but the morphology appears more similar to clusters of bentonite. The 2000x shows how the filaments are characterized by the presence of pores in the range of 10-20µm. A detail of an approximately 15 um pore with 200X magnification [ma controlla, secondo me qui intendi la 2000X] suggests that they are generated by the passage of a gas, possibly water vapour during the drying stage, as the edges are faced outwards with smooth walls.

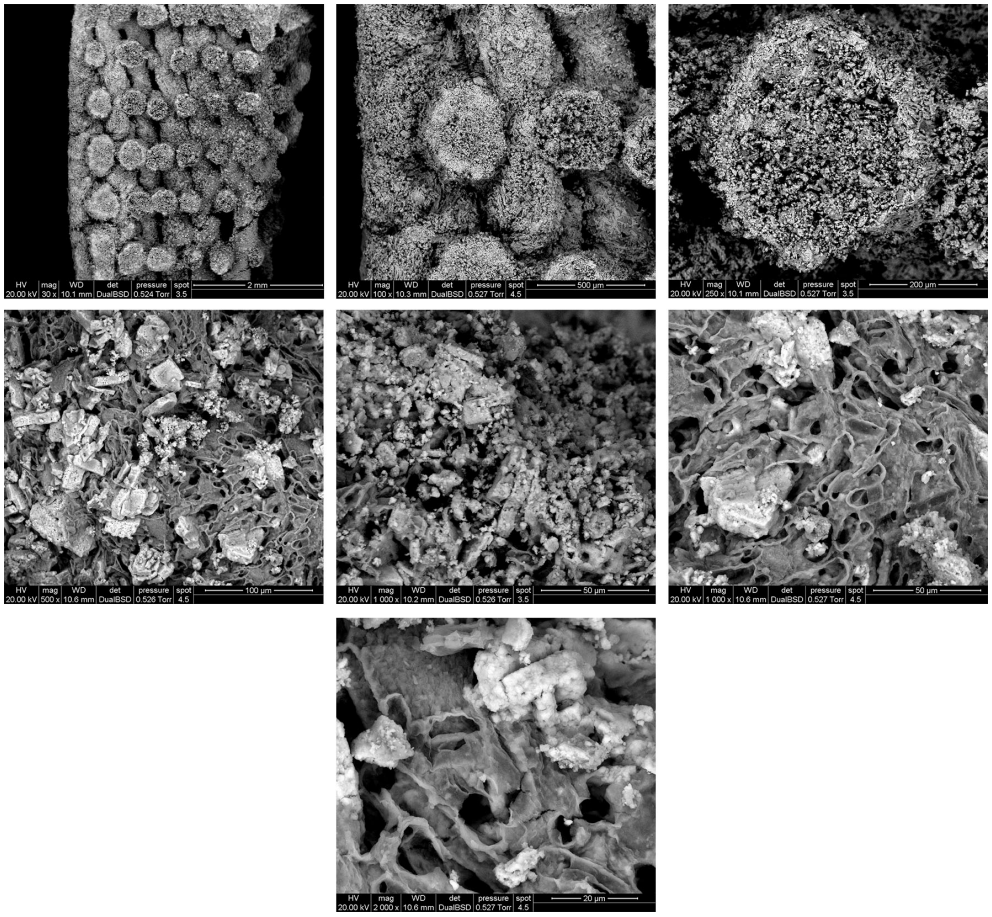

Figure 3.23: 70%NOHT composition, from top left to right: 30x, 100x, 250x, 500x, 1000x, 1000x, 2000x

The second set of images presented are ones of the 70% composition but focusing instead on the external surface of the filament. Similarities are present with the fracture surface morphology of the previews set of images, but the samples also display a number of new features. As before there is a presence of scattered lamellar structuress with smooth surface that can be associated with the presence of bentonite. At higher magnifications the $SrCl_2$ appear likes more regularly shape crystals and not random clusters, this can be associated to a process of dissociation and recrystallization of the salt, as the powder used was spherically shaped. To identify the salt elongated shapes that show superficial roughness or small particulates on the surface should be considered such as those prominently shown in the last image. Looking at the pore distributions the side shot does not show the presence of many little pores like for the section of the filaments, but a large pore of about 40µm can be seen in one of the pictures.

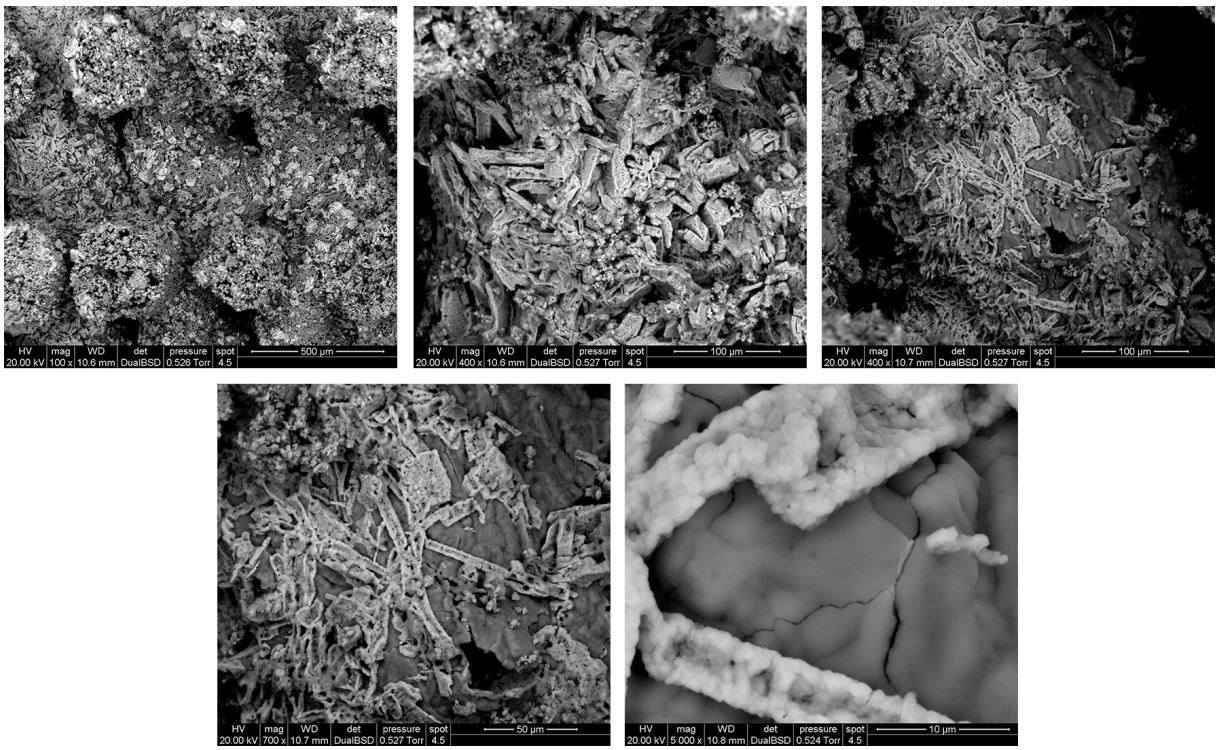

Figure 3.24: 70%NOHT composition, from top left to right: 100x, 400x, 400x, 700x, 5000x

3.6.3 70% composition HT

The third set of images presented are the ones of the 70% composition but after heat treatment which was found to induce a drastic change in the microstructure. The whole external surface of the filaments is characterized by the presence of well defined needle like structures and small edgy clusters with flakes. The needles form something that looks like a web that covers all the surface while others reach out from inner layers denoting that the needles are present both inside and outside the filaments. The thermal treatment likely induce a phase change in the strontium chloride and bentonite matrix that produces such needles which propagate and close up all the pores reducing surface area. Between the needles small platelets associated with the possible presence of bentonite can be observed. The morphology of the surface is overall reminescent of a bramble.

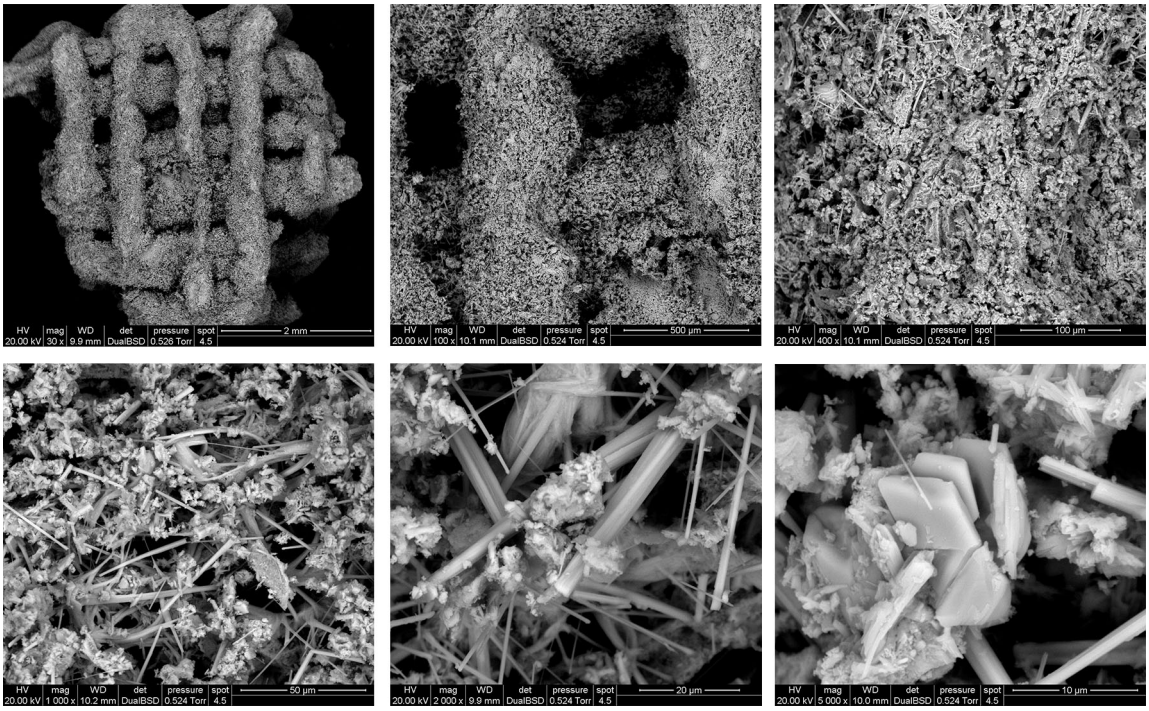

Figure 3.25: 70%NOHT composition, from top left to right: 30x, 100x, 400x, 1000x, 2000x, 5000x

The fourth set of images presented are ones of the 70% HT but with focus on the section of the filament, the structure does not appear particularly different from the top section. The images still clearly show the needle-shaped crystals that envelope all the filaments from the inner to the outer layer. It must be noted that differently from the sections of the untreated samples there are no visible inhomogeneities in crystal morphology. The surface of the sections appears extremely rough, the whole area is packed with needles and cluster, despite the visual appearance of a high degree of porosity, its dimensions are far too large to add any significant contribution to the BET SSA which remains dominated by the absence of mesoporosity in this sample. A detail of the needle-shaped structures can be seen in the last image.

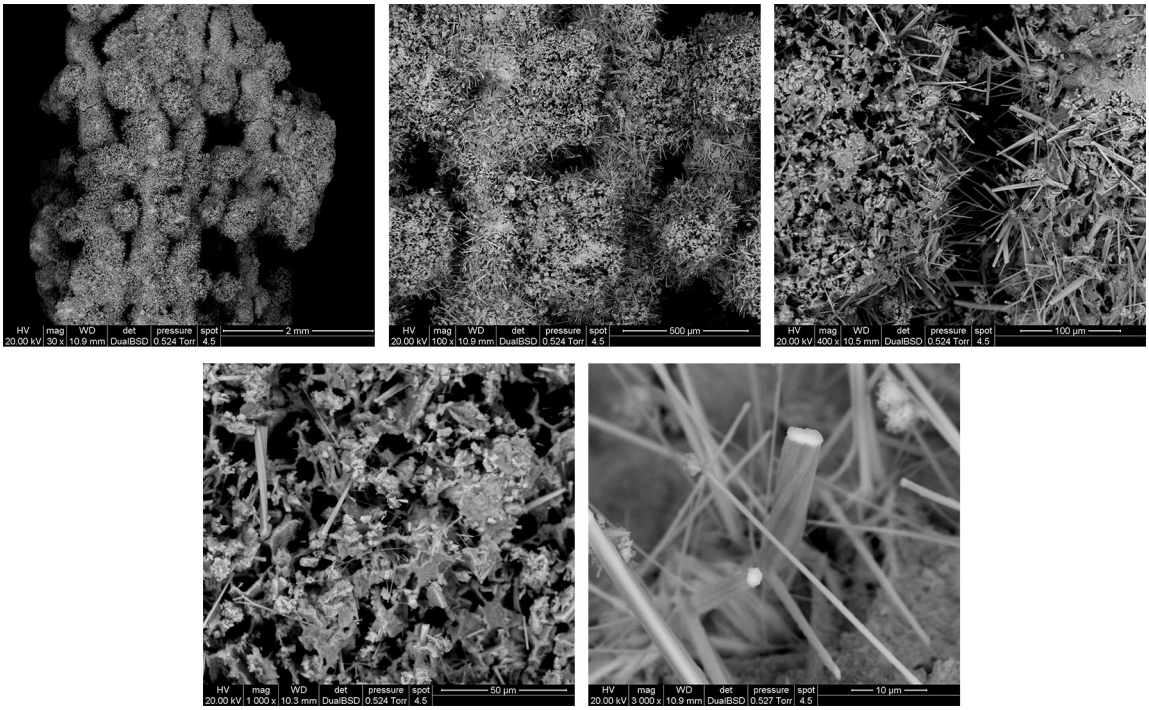

Figure 3.26: 70%HT composition, from top left to right: 30x, 100x, 1000x, 3000x

3.6.4 60% composition

The fifth set of images presented are those of the 60% composition, the micrographs were collected with a different apparatus than the 70% composition, and only SE imaging was performed. The structure looks consistent with the ones of the 70% without heat treatment sample as the side of the filaments again shows clusters of the strontium chloride salt, while at the sections of the filaments a more homogeneous phase can be connected to the presence of bentonite, as in a similar SEM images found in literature [17]. The surface overall displays a considerably lower amount of visible porosity compared to the 70% composition.

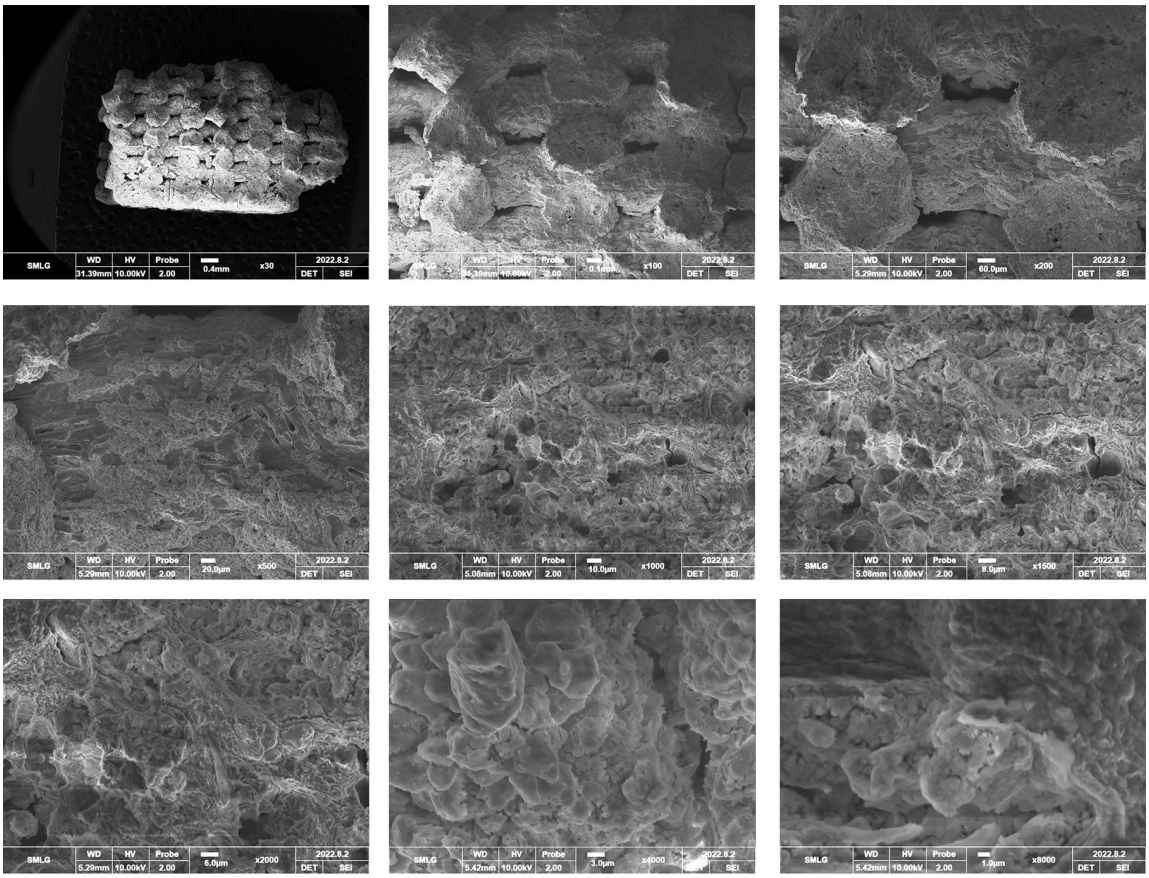

Figure 3.27: 60% composition, from top left to right: 30x, 100x, 200x, 500x, 1000x, 1500x, 2000x, 4000x, 8000x

3.6.5 80% composition

The sixth and last set of images presented are ones of the 80% composition, it is clearly evident that the mechanical test completely destroyed the integrity of structure, as not many defined filaments are visible and the whole surface appears like packed powder. All the image were taken on the left side, with particular interest to the morphology of the fracture sections. The surface morphology is very different from the 60% composition showing a visible crust-like appearance which is most likely related to the increase in strontium chloride, but without backscattering it is difficult to give a precise estimate about the origin of this phase, most likely is a mix of bentonite and strontium chloride.

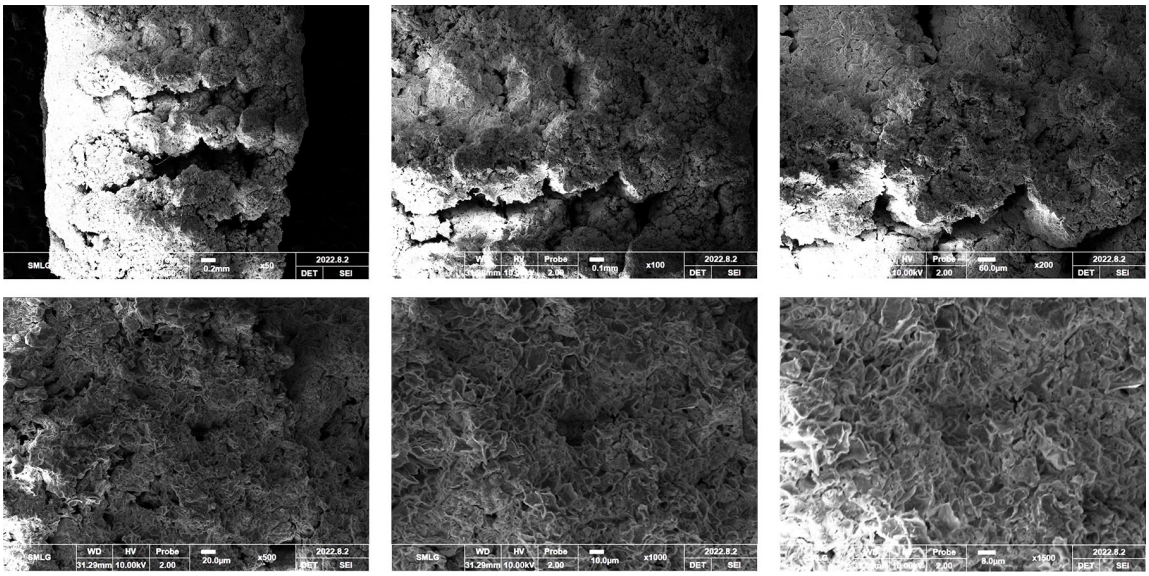

Figure 3.28: 80% composition, from top left to right: 50x, 100x, 200x, 500x, 1000x, 1500x

Summarizing all the images, it is possible to understand how the two component interacts with or without heat treatment and how the microstrucure changes according to the variation in concentration.

The main results of the SEM analysis are as follows:

- homogeneous matrix made of strontium chloride and bentonite;
- clusters of strontium chloride or bentonite of different shape;
- the HT produces the appearance of a needle phase;
- as the % of strontium chloride content is increased, the microstrucutre becomes more consistent and only the presence of a mixed phase, with the disappearance of the clusters and the platelets;
- as the % of strontium chloride is decreased the filaments are more dense and the microstructure is less dishomogeneous.

APPENDIX A

Weibull data

B1	B2	B3	H1	H2	Davg[mm]	Havg[mm]	A[mm^2]	Load[N]	σ[MPa]
9,36	9,24	9,40	3,76	3,75	9,33	6,55	68,42	169,77	2,48
10,08	9,74	10,66	4,10	4,02	10,16	7,13	81,07	140,00	1,73
8,12	8,33	9,11	3,82	3,73	8,52	6,17	57,01	170,00	2,98
9,20	8,60	10,16	4,29	4,45	9,32	6,81	68,22	126,37	1,85
9,21	8,81	10,05	4,10	4,16	9,36	6,73	68,76	126,71	1,84
9,54	9,21	10,00	4,08	4,03	9,58	6,83	72,13	131,00	1,82
8,92	9,05	10,02	3,76	3,66	9,33	6,55	68,37	55,80	0,82
9,56	9,39	9,79	3,62	3,74	9,58	6,60	72,08	86,68	1,20

Table A.1: 70% composition, heat treatment 800°

B1	B2	B3	H1	H2	Davg[mm]	Havg[mm]	A[mm^2]	Load[N]	σ[MPa]
9,59	10,08	9,88	4,17	4,09	9,85	4,13	76,20	102,00	1,34
9,36	9,50	9,95	4,18	4,00	9,60	4,09	72,43	100,00	1,38
9,23	9,15	9,79	4,38	4,45	9,39	4,42	69,25	80,13	1,16
9,63	9,45	10,01	4,35	4,26	9,70	4,31	73,85	84,00	1,14
10,07	9,67	9,93	4,32	4,36	9,89	4,34	76,82	93,00	1,21
9,93	10,03	9,73	4,08	4,26	9,90	4,17	76,93	91,00	1,18
9,50	10,21	10,32	4,27	4,21	10,01	4,24	78,70	112,00	1,42
9,56	9,39	9,79	3,62	3,74	9,58	6,6	72,08	86,68	1,20

Table A.2: 70% composition

B1	B2	B3	H1	H2	Davg[mm]	Havg[mm]	A[mm^2]	Load[N]	σ[MPa]
9,97	9,27	9,60	4,63	4,67	9,61	4,65	72,58	168,38	2,32
10,13	10,43	9,76	4,16	4,19	10,11	4,18	80,22	204,88	2,55
9,29	9,20	9,02	4,77	4,45	9,17	4,61	66,04	291,63	4,42
9,21	9,25	9,38	4,68	4,57	9,28	4,63	67,64	300,00	4,44
9,67	9,30	9,53	4,55	4,34	9,50	4,45	70,88	430,00	6,07
9,82	9,87	9,98	4,12	4,32	9,89	4,22	76,82	305,00	3,97
9,73	9,92	9,85	3,99	3,95	9,83	3,97	75,94	294,54	3,88
9,41	9,67	9,61	4,84	4,78	9,56	4,81	71,83	120,85	1,68
9,19	9,70	9,58	4,22	4,14	9,49	4,18	70,73	224,48	3,17
9,16	9,53	9,27	4,13	4,41	9,32	4,27	68,22	212,15	3,11
9,72	9,80	9,82	4,14	4,40	9,78	4,27	75,12	150,77	2,01
9,45	9,70	9,23	4,47	4,46	9,46	4,47	70,29	356,40	5,07
9,47	9,41	9,37	3,79	3,80	9,42	3,80	69,64	224,00	3,22
9,75	9,36	9,60	4,23	4,16	9,57	4,20	71,93	172,00	2,39
9,63	9,51	9,67	4,42	4,36	9,60	4,39	72,43	698,96	9,65

Table A.3: 60% composition

B1	B2	B3	H1	H2	Davg[mm]	Havg[mm]	A[mm^2]	Load[N]	σ[MPa]
10,24	10,23	10,31	4,59	4,32	10,26	4,46	82,68	18,72	0,23
10,57	10,40	10,32	4,48	4,69	10,43	4,59	85,44	10,43	0,12
9,92	10,20	10,06	4,83	4,90	10,06	4,87	79,49	34,05	0,43
10,55	10,25	10,50	4,43	4,23	10,43	4,33	85,49	25,58	0,30
9,90	9,85	9,70	4,08	4,24	9,82	4,16	75,69	12,82	0,17
9,94	9,92	10,08	4,45	4,24	9,98	4,35	78,23	33,15	0,42
10,48	10,38	10,35	4,14	4,69	10,40	4,42	85,00	6,60	0,08
10,71	10,23	10,20	4,29	4,33	10,38	4,31	84,62	6,48	0,08
9,96	10,52	10,51	4,20	4,26	10,33	4,23	83,81	12,03	0,14
10,60	10,53	10,54	5,02	5,34	10,56	5,18	87,53	18,79	0,21
10,43	10,22	10,35	4,57	4,61	10,33	4,59	83,86	29,41	0,35
10,32	10,05	10,22	4,07	4,03	10,20	4,05	81,66	39,05	0,48
10,50	10,30	10,45	4,44	4,53	10,42	4,49	85,22	7,30	0,09
10,03	9,64	10,32	4,38	4,50	10,00	4,44	78,49	9,51	0,12
10,39	10,50	9,76	4,54	4,70	10,22	4,62	81,98	17,94	0,22
10,90	10,40	10,50	4,95	4,76	10,60	4,86	88,25	15,25	0,17

Table A.4: 80% composition

	70-30 HT			
j	Ranked stress [MPa]	S	lnσ	ln(ln1/S)
1	0,816170757	0,9375	-0,20313	-2,74049
2	1,202535769	0,8125	0,184432	-1,57195
3	1,726834586	0,6875	0,54629	-0,98165
4	1,816135408	0,5625	0,596711	-0,55275
5	1,84280208	0,4375	0,611287	-0,19034
6	1,852346715	0,3125	0,616453	0,151133
7	2,481404206	0,1875	0,908825	0,515202
8	2,981809201	0,0625	1,09253	1,019781

Table A.5

	70-30 NOHT			
j	**Ranked stress [MPa]**	**S**	**lnσ**	**ln(ln1/S)**
1	1,137481839	0,928571	0,128817	-2,60223
2	1,157108481	0,785714	0,145924	-1,42229
3	1,182969712	0,642857	0,168028	-0,81682
4	1,210599483	0,5	0,191116	-0,36651
5	1,338559958	0,357143	0,291594	0,029189
6	1,380594413	0,214286	0,322514	0,432071
7	1,423180506	0,071429	0,352894	0,970422

Table A.6

	60-40			
j	**Ranked stress [MPa]**	**S**	**lnσ**	**ln(ln1/S)**
1	1,682434581	0,966667	0,520242	-3,38429
2	2,006999868	0,9	0,696641	-2,25037
3	2,319811095	0,833333	0,841486	-1,70198
4	2,391193327	0,766667	0,871793	-1,32538
5	2,553840675	0,7	0,937598	-1,03093
6	3,10972031	0,633333	1,134533	-0,7836
7	3,173623092	0,566667	1,154874	-0,56566
8	3,216353258	0,5	1,168248	-0,36651
9	3,878402505	0,433333	1,355423	-0,17883
10	3,970245615	0,366667	1,378828	0,003297
11	4,415741536	0,3	1,485176	0,185627
12	4,435426847	0,233333	1,489624	0,375203
13	5,070672261	0,166667	1,623473	0,583198
14	6,066404479	0,1	1,802766	0,834032
15	9,649802708	0,033333	2,266937	1,224128

	80-20			
j	**Ranked stress [MPa]**	**S**	**lnσ**	**ln(ln1/S)**
1	0,076575602	0,96875	-2,56948	-3,4499
2	0,077644201	0,90625	-2,55562	-2,31831
3	0,085659482	0,84375	-2,45738	-1,77255
4	0,121165844	0,78125	-2,1106	-1,39893
5	0,122074741	0,71875	-2,10312	-1,10793
6	0,14357651	0,65625	-1,94089	-0,86462
7	0,169383091	0,59375	-1,77559	-0,65144
8	0,172809746	0,53125	-1,75556	-0,45804
9	0,214675895	0,46875	-1,53863	-0,27749
10	0,218833652	0,40625	-1,51944	-0,10449
11	0,226423366	0,34375	-1,48535	0,065639
12	0,299202001	0,28125	-1,20664	0,237844
13	0,350690713	0,21875	-1,04785	0,418596
14	0,423772303	0,15625	-0,85856	0,618584
15	0,428382059	0,09375	-0,84774	0,861676
16	0,47820566	0,03125	-0,73771	1,242925

Table A.7

Conclusions

The aim of the project was to design, produce and characterize structured ammonia sorbents based on strontium chloride using the 3D printing technique of Direct ink Writing. During the experimentation three different ink were implemented, each with a different concentration of the raw materials: specifically 60-70-80% of Strontium Chloride were used and mixed with bentonite. As the ink was optimized the structured sorbents were printed and characterized. A single porous lattice design was used for all the composition.

The 70% composition unlike the others underwent heat treatment to enhance the mechanical properties of the structure, different observation were made based on the results obtained:

- Sorbtion data of the treated samples were underwhelming, while the ones of the untreated ones were in line with the expectations, as the structure was able to adsorb 600 mg/g (37,8 mmol), but it was not able to withstand the asorption cycles, reaching fracture at the 6th one;
- the uniaxial compression test show how the treated sample performed better by having a Weibull modulus higher of the untreated sample, m of 12,1 while the untreated ones 2,9;
- EDS showed how larger sal crystals form on the outer layers of the filaments in the untreated composition, due to different crystallization kinetics made possible by differential evaporation and evaluated the composition of the needle shaped crystals in the treated ones suggesting they may be associated with a mixed phase formed at high temperature;
- SEM shows how the treated samples undergo a drastic microstructural evolution during heating;
- XRD showed that the pattern of the untreated 3D printed sample is comparable to that of the starting powder mixture, underlying the fact that it was indeed the heat treatment which changed the phase composition and microstructure, producing peaks related to the appearance of probable strontium alluminoslicates.

The 60% and the 80% were not evaluated for the sorbtion ammonia analysis, but it can be expected that the uptake of the 80% would be increased at expense of the structural stability, meaning that failing would happen at lower cycles, while for the 60% the opposite would hold true. Nonetheless, both the compositions were characterized by other techniques. Both composition underwent SEM analysis on a different apparatus than the 70%, that did not have an EDS analyzer. The 60% composition yielded these results:

- mechanical performance was enhanced by the higher concentration of bentonite as the fracture stress achieved was the maximum among all the compositions, the structure was characterize by a Weibull modulus of 2,58 and scale factor of 4,3;
- SEM images show how the microstructure was more homogeneous and dense;
- XRD, just like the 70% composition the 60% did not show the appearance of new phases after printing.

For the 80% composition on the other hand:

- the structure showed very poor mechanical performance, not being able to resist even small loads, showing low Weibull modulus of 1,94 and scale factor of 0,26. This was the lowest value achieved for all compositions.;
- SEM images denoted an homogeneous phase made of the mix of bentonite and strontium chloride;
- XRD, as for the 70% composition did not show new phases after printing similarly the 60%.

The composites offer good characteristics, such as a wide range of strontium chloride loading and a possible structure for the volume expansion. The cavities in the porous structure and the good SSA of the networks provide a selfregulating environment for strontium chloride during ammonia absorption and desorption.

Bibliography

[1] Cheremisinoff N. P. Handbook of air pollution prevention and control. pages 1–560, 2002. (Cited at page 1)

[2] Clean Air Technology center (MD-12). Nitrogen oxides (nox), why and how they are controlled. pages 1–41, 1999. (Cited at page 1)

[3] Bracco P. Cremonini R. Ravina M. Robotto A., Barbero S. and Brizio E. Improving air quality standards in europe: Comparative analysis of regional differences, with a focus on northern italy. *Atmosphere*, 13(642):1–18, 2022. (Cited at page 2)

[4] Miljøstyrelsen V. Guidelines for air emission regulation: Limitation of air pollution from installations. *Environmental Guidelines*, (1):10–117, 2002. (Cited at page 2)

[5] Sadashiva Prabhu S. A review on selective catalytic reduction (scr)-a promising technology to mitigate nox of modern automobiles. *International Journal of Applied Engineering Research*, 13(1):5–9, 2018. (Cited at page 3)

[6] Elsener M. Mehring M. and Kröcher O. Diesel soot catalyzes the selective catalytic reduction of nox with nh3. *Topics in Catalysis*, 56:440–445, 2013. (Cited at page 4)

[7] photo took from https://eurol.com/en/what-is-the-function-of-adblue/. (Cited at page 4)

[8] Udell K. S. Mofidi S. A. H. Study of heat and mass transfer in mgcl2/nh3 thermochemical batteries. *Journal of Energy Resources Technology*, 139(3):032005–1 – 032005–10, 2017. (Cited at page 5)

[9] Luukkonen T. Bai C. Scanferla P. Botti R. Carturan S. Innocentini M. Franchin G., Pesonen J. and Colombo P. Removal of ammonium from wastewater with geopolymer sorbents fabricated via additive manufacturing. *Materials Design*, 195:109006, 2020. (Cited at page 14)

[10] Das A. Griggs C. S. Klaus K. Kennedy A. J., Ballentine M. L. and Bortner M. J. Additive manufacturing for contaminants: Ammonia removal using 3d printed polymer-zeolite composites. *ACS EST Water*, 1(3):621–629, 2021. (Cited at page 14)

[11] Neimark A. V. Olivier J. P. Rodriguez-Reinoso F. Rouquerol J. Thommes M., Kaneko K. and Sing K. S. W. Physisorption of gases, with special reference to the evaluation of surface area and pore size distribution (iupac technical report). *Pure and Applied Chemistry*, 87(9-10):1051–1069, 2015. (Cited at pages 16 e 26)

[12] Baumann M.J. Fan X., Case E.D. Weibull parameters and the tensile strength of porous phosphate glass-ceramics. *journal of the mechanical behavior of biomedical materials*, 20(12):283–295, 2013. (Cited at page 35)

[13] Frederic B. Lucien D. Francois P., Pascal E. Weibull parameters and the tensile strength of porous phosphate glass-ceramics. *Ceramic society*, 82(3):641–648, 1999. (Cited at page 35)

[14] Zhao S. Liang W., Xu S. Experimental study of temperature effects on physical and mechanical characteristics of salt rock. *Rock Mech. Rock Engng*, 39(5):469–482, 2006. (Cited at page 36)

[15] Sun Y. Song X. Yu J. Quian Y., Lu G. Preparation of strontium chloride hexahydrate by batch-cooling crystallization: Control of crystal size and morphology. *Crystal Research and Technology*, 49(11):878–887, 2014. (Cited at page 37)

[16] Muserreff O. Aktham A. Dale Eric W. Umran Dogan A., Meral D. Baseline studies pf the clay minerals society source clays: specific surface area (bet) method. *Clays and Clay Minerals*, 54(1):62–66, 2006. (Cited at page 46)

[17] Marey A. Composite of chitosan and bentonite as coagulant agents in removing turbidity from ismailia canal as water treatment plant. *Revista Bionatura*, 4(3):897–900, 2019. (Cited at page 55)

Sitografia

- Chemical Book – `www.pubchem.ncbi.nlm.nih.gov`
- Chemical Book – `www.chemicalbook.com`
- Sigma Aldrich – `www.sigmaaldrich.com`
- Wikipedia – `www.wikipedia.org`